J. Fluid Mech. (1996), *vol.* 322, *pp.* 297–328

Turbulence measurements around a mild separation bubble and downstream of reattachment

By AMY E. ALVING[1] AND H. H. FERNHOLZ[2]

[1]Aerospace Engineering & Mechanics, University of Minnesota, Minneapolis, MN 55455, USA

[2]Hermann-Föttinger Institut, Technische Universität Berlin, Germany

(Received 24 January 1994 and in revised form 5 April 1996)

This paper describes the behaviour of a turbulent boundary layer on a smooth, axisymmetric body exposed to an adverse pressure gradient of sufficient strength to cause a short region of mean reverse flow ('separation'). The pressure distribution is tailored such that the boundary layer reattaches and then develops in a nominally zero pressure gradient. Hot-wire and pulsed-wire measurements are presented over the separated region and downstream of reattachment. The response of the turbulence quantities to separation and to reattachment is discussed, with emphasis on the relaxation behaviour after reattachment. Over the separation bubble, the response is characteristic of that seen by other workers: the Reynolds stresses in the inner region are reduced and stress peaks develop away from the wall. At reattachment, the skewness of the fluctuating wall shear stress vanishes, as it is known to do at separation. After reattachment, the outer-layer stresses decay towards levels typical of unperturbed boundary layers. But the inner-layer relaxation is unusual. As the viscous wall stress increases downstream of reattachment, the recovery does not start at the wall and travel outward via the formation of an 'internal' layer, the process observed in many other relaxing flows. In fact, the inner layer responds markedly more slowly than the outer layer, even though response times are shortest near the wall. It is concluded that the large-scale, outer structures in the turbulent boundary layer survive the separation process and interfere with the regeneration of Reynolds stresses in the inner region after reattachment. This behaviour continues for at least six bubble lengths (20 boundary-layer thicknesses) after reattachment and is believed to have profound implications for our understanding of the interaction between inner and outer layers in turbulent boundary layers.

1. Introduction

The separation of a wall shear layer is important in many technological applications, often because it causes severe losses and performance degradation. Separation caused by step changes in surface geometry is present at all Reynolds numbers, while adverse-pressure-gradient (APG)-induced separation from smooth surfaces depends strongly on the Reynolds number in addition to the magnitude and duration of the pressure gradient. This means that the flow over a smooth surface may separate under some combinations of parameters (pressure gradient, speed, curvature, etc.) but not under others, and it is of obvious interest to be able to understand and predict these differences. Several studies have examined the mean-flow behaviour of wall shear

layers at and around APG-induced separation, beginning with Stratford's (1959*a*,*b*) classic zero-skin-friction (incipient separation) study, followed by Townsend's (1961), Perry & Schofield's (1973) and Schofield's (1981, 1986) studies of published data, and by Melnik's (1989, 1991) and Durbin & Belcher's (1992) asymptotic analyses. Recent experimental investigations include Dengel & Fernholz (1990) and Driver (1991), two similar investigations of the sensitivity of separation to the pressure-gradient history. Most of these works concentrated on scaling the mean-velocity profile as the friction velocity goes to zero and on predicting the profile computationally, but the last two include fairly complete sets of turbulence measurements. The extreme sensitivity of the location of separation to the imposed pressure gradient has been shown by Stratford (1959*a*,*b*), by Spangenberg, Rowland & Mease (1967), and by Dengel & Fernholz (hereinafter referred to as DF), with the implication that computations will be difficult in such flows. Driver (1991) and Menter (1992) discuss the degree and accuracy with which various turbulence-closure models can predict flows close to separation; the former's results show that even models which can perform well up to and over the separated region break down near reattachment – that is, reattachment seems to be a 'harder' problem computationally than separation. The inverse formulation has been shown to be successful (Schalau, Thiele & Dengel (1989)) but requires the distribution of the displacement thickness be prescribed, information which may not be available to the computationalist.

Neither DF nor Driver continued their measurements downstream of reattachment, so no experimental results are available for a wall shear layer relaxing from reattachment after a mild, APG-induced, closed reverse-flow region. This topic is important because many engineering devices operate close to the onset of separation, since they are in some sense most efficient there. For instance, Stratford's work was motivated by the task of creating a diffuser as short as possible by maintaining the skin friction at zero over a finite length. Similarly, the maximum lift on an airfoil occurs near the onset of separation. Thus it is important to understand how the flow behaves in the event that a device operates in the presence of a mild separation bubble surrounded upstream and downstream by wall-attached flow. The aim of the present study is to investigate such a flow, concentrating especially downstream of the reattachment location.

A description of a 'mild' separation is in order here. A distinction has already been made between geometry-induced and APG-induced separations, which have two important physical differences: (i) in the former case, one edge of the separation bubble is fixed at the step change in surface geometry, whereas both the leading and trailing edges of the bubble are free to move about over time in the latter; and (ii) the bubble height in the former case is typically larger than the thickness of the separating shear layer, so that the strong shear layer which results grows initially independently of the wall below the bubble. In the case of a 'strong' APG-induced separation, the bubble height is on the order of the same thickness as the pre-separation shear layer, while by 'mild' we mean the bubble height is significantly less than this. Strong separations often have an added degree of complexity in that the separated shear layer may not reattach to the test surface. Such 'open-bubble' flows have been studied somewhat more than the type which is the topic of this work, most notably in a series of experiments by Simpson and co-workers (Shiloh, Shivaprasad & Simpson (1981) and Simpson, Chew & Shivaprasad (1981*a*,*b*). The behaviour of strong separations is in some ways very different from that of the mild separations of interest here. For instance, Simpson *et al.* have shown the existence of a new scaling law for the backflow under the large bubbles where the reverse flow is strong, and this scaling

does not apply here. But some results are relevant to all APG-induced separations, such as the fact that the mean streamline pattern around the bubble is unrelated to instantaneous particle paths and is therefore misleading. They state, "... backflow does not come from far downstream as suggested in [the mean-streamline picture], but appears to be supplied intermittently by large-scale structures as they pass through the separated flow..." (Simpson *et al.* 1981*b*). It is likely that a similar unsteady mechanism is present in the case of a mild separation bubble, so that this concept should be kept in mind for understanding the current work.

The present experimental investigation can be viewed along the lines of a continuation of the work of DF; indeed, the same flow facility and instrumentation were used. DF allowed a turbulent boundary layer to grow along an axisymmetric test surface and adjusted the pressure gradient to result in instantaneous reverse flow over the last third of the test area. They studied three cases of slightly different pressure gradient such that, over the region of instantaneous reverse flow, the skin friction was approximately zero, slightly positive, or slightly negative – the last case (Case 3) being the mild separation. The experiment done by Driver (1991) is qualitatively similar to that of DF, even to the extent that Driver also used an axisymmetric test surface (although in a rectangular cross-section) for which the transverse curvature was about the same strength as in this work. Driver, however, concentrated heavily on using the experimental results to evaluate turbulence models, a topic not addressed in this paper. The work described in this paper is similar to the mild separation of Case 3 in DF, with the main differences being that the separation in the current study occurs much farther upstream and that the motivation here is to study the process of relaxation from reattachment. The purpose of this paper is to present the turbulence measurements and discuss them in the light of our current understanding of turbulent boundary-layer structure. Although the emphasis is on the relaxation behaviour, the measurements up to and including separation are also presented, to provide the reader with an understanding of the 'perturbation' from which the boundary layer is recovering and to comment on a few open issues in the literature. In addition, in the present experiment the boundary layer is tripped in a region of APG, and the results obtained through separation prove that this flow separates in qualitatively the same way as boundary layers which originate in a zero pressure gradient (ZPG) before experiencing APG. This observation provides support for the expectation that the relaxation behaviours should also be qualitatively similar.

A companion paper, Alving & Fernholz (1995, here referred to as AF), discusses the scaling of the mean velocity profile in turbulent boundary layers around the separation bubble and after reattachment. The most important results presented in that paper are summarized in §3 for the convenience of the reader.

2. Experimental arrangement and measuring techniques

The facility used in this experiment is shown in figure 1 and is similar to that described in DF (1990), with minor modifications as discussed here. The test surface was a new hollow aluminium circular cylinder, 1.65 m in length and 0.25 m in diameter, its axis aligned with the flow and preceded by a 0.3 m elliptical nosecone. The boundary layer was tripped at the nosecone/cylinder junction using a Dymo tape of raised V's. The test surface was surrounded by a concentric, perforated cylinder forming the outer wall (diameter 0.61 m) and ended at a perforated end plate.

The wind tunnel was the same open-return, blower facility described in DF. Air entered through a non-woven filter mat, passed through a 12 kW centrifugal fan,

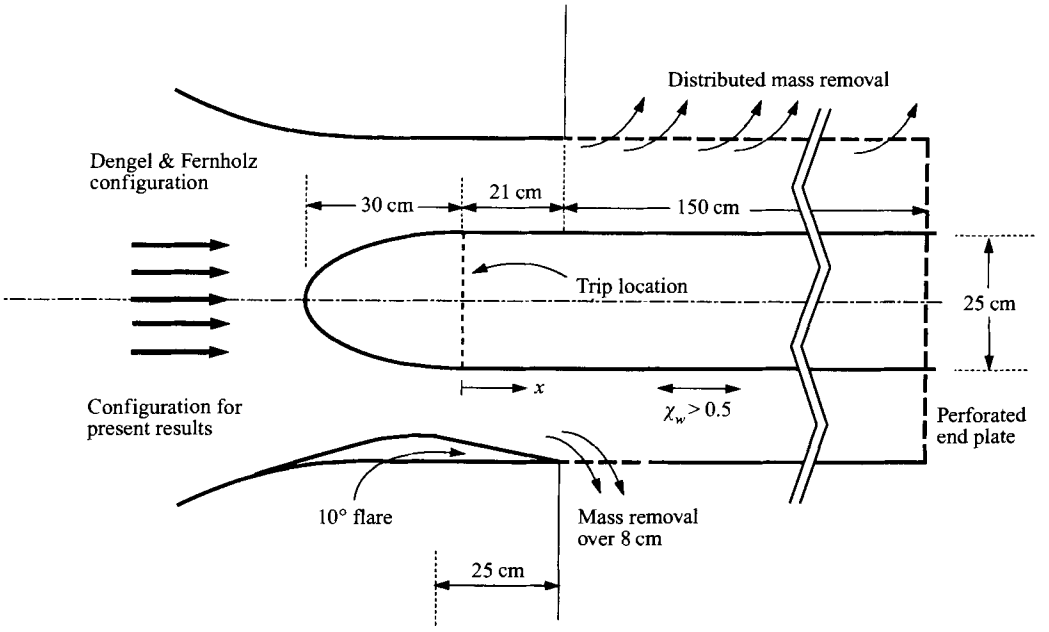

FIGURE 1. Sketch of the facility.

and entered a 2.0 m long, 2.0 m diameter, circular-cross-section settling chamber. The upstream end had a single, precisely manufactured, perforated metal plate (64% openness) to improve the flow uniformity. An axisymmetric nozzle followed the settling chamber, and near the end of the contraction the flow encountered the nosecone and test surface. For this work, the original DF contraction was modified slightly with a fibreglass insert to over-contract, then re-expand, the cross-section to start the adverse pressure gradient as far upstream as possible. For comparison, figure 1 shows both the DF configuration (top half of diagram) and that used in the present work (bottom half). In each case, the geometry was axisymmetric, with the chain-dotted line showing the axis of rotational symmetry. In this investigation, the contraction ratio of the nozzle (plus insert) was 18.9:1 at the throat, just after which the nozzle wall diverged at 10° over the next 0.25 m to give a net contraction of 12.8:1 for the rest of the test section. To prevent separation on the flared nozzle wall, its boundary layer (not the test boundary layer) was tripped just upstream of the throat with 5 mm diameter copper tubing. Flow visualization using very fine tufts showed that the flow remained attached over the nozzle wall. Downstream of the flare, some of this outer-wall boundary layer was removed through the porous outer wall (see below). The turbulence intensity at the inlet to the test section $\overline{u^2}^{1/2}/U_{throat}$ was 0.2% and the mean-velocity distribution near the throat was uniform to within $\pm 0.3\%$.

The streamwise pressure gradient was tailored to create a small separation bubble as far upstream as possible (much earlier than in the DF case) to allow observation of the downstream reattachment/relaxation behaviour. The bubble location and size were determined by the nozzle flare, the degree of perforation of the end plate (53%), and the perforation of the outer wall. This last was 38% porous over the first 80 mm, while the remainder of the perforations were covered with impermeable adhesive plastic.

The arrangement described above led to the streamwise static pressure distribution

shown in figure 2(*a*). The streamwise coordinate, ξ, is the distance from reattachment (occurring at x_{reatt}), non-dimensionalized by the length of the bubble, $\ell = x_{reatt} - x_{sep}$:

$$\xi = \frac{x - x_{reatt}}{\ell}. \tag{1}$$

A single, movable tap was used so that successive pressure measurements were unaffected by small variations in the surface near the tap, by the tube length, etc. The tap was in a plug which fitted into a streamwise slot of 20 mm width milled along the length of the test surface. As a refinement over the DF facility, the surface of these interchangeable plugs had the same transverse radius of curvature as the rest of the cylinder, to remove the possibility of flat plug surfaces affecting wall measurements. Static pressure was referenced to that at the throat, measured with a Pitot-static tube in the free stream located 180° around the circumference from the measuring position. The free-stream unit Reynolds number at the throat was constant at $1.62 \times 10^6\ \mathrm{m^{-1}}$ ($U_{throat} \simeq 25\ \mathrm{m\,s^{-1}}$).

The three components of the fluctuating velocity were measured using single and crossed hot-wire probes wherever possible. The crossed-wire probes had a cage face of 1.5 mm × 0.7 mm and are described in Dengel (1992). Pulsed wires were used in regions of reverse flow or high turbulence intensity where hot wires are not valid; pulsed-wire anemometry is described, for example, in Bradbury & Castro (1971). The sensing wires of the traversing pulsed-wire probe (Jaroch (1985)) stretched 6 mm in the spanwise direction and measured only the streamwise component of velocity fluctuations, because the inclined pulsed wires required for v^2 and $-\overline{uv}$ measurements give unacceptably inaccurate data: Dengel (1992) estimates the pulsed-wire uncertainty for $\overline{u^2}$ at better than ±5%, for $-\overline{uv}$ at ±20%, and for $\overline{v^2}$ at ±30%. The streamwise component of the fluctuating wall shear stress was measured with two wall-mounted pulsed-wire probes calibrated in zero pressure gradient against a Preston tube; the probe with the more closely spaced wires was used in and around the separation bubble (325 mm $\leqslant x \leqslant$ 625 mm), while the one with wires spaced farther apart was used everywhere else. The wall pulsed-wire probes were each integrated into one of the interchangeable plugs described above and the wires were 0.03 mm away from the wall in both cases. Both the wall-mounted and the traversing pulsed-wire probes also gave the probability of reverse flow at the measuring point.

The hot-wire anemometer was an AA Systems constant-temperature anemometer with the high-frequency option (square-wave-test response in excess of 100 kHz). The pulsed-wire anemometer was built in-house (Wagner 1986). Data acquisition was achieved using Rhotron hardware controlled by an Atari microcomputer. The probes were traversed away from the wall using an electrically driven gear with an incremental resolution of 0.005 mm. Probe access was through a slot in the wall of the outer cylinder.

DF showed that a separation bubble of the sort studied here (small in size, induced by an adverse pressure so the position of onset is not firmly fixed) is extremely sensitive to small variations in its environment. This is a significant advantage of the cylindrical test surface: the absence of sidewall boundary layers removes an important source of three-dimensionality. In addition, great care was taken to ensure that the free stream was as uniform as possible in the circumferential (spanwise) direction (see Dengel & Fernholz 1989). A plot of the circumferential skin-friction distribution at several streamwise locations is shown in figure 3 (the boundary-layer profiles were measured at 0°). This plot shows that the flow approaches separation ($C_f = 0$) fairly uniformly and that irregularities in the young (pre-separation) boundary layer

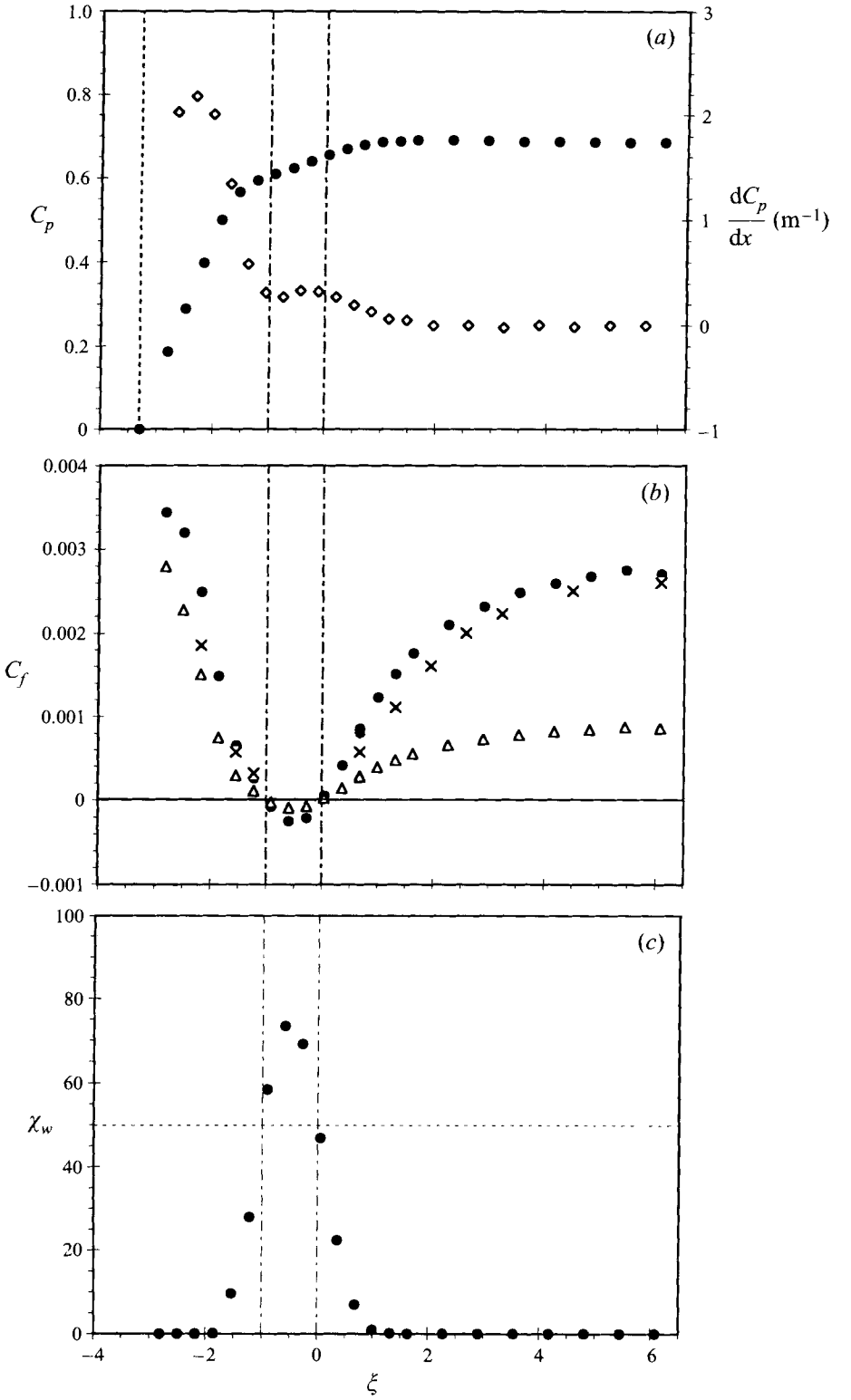

FIGURE 2. For caption see facing page.

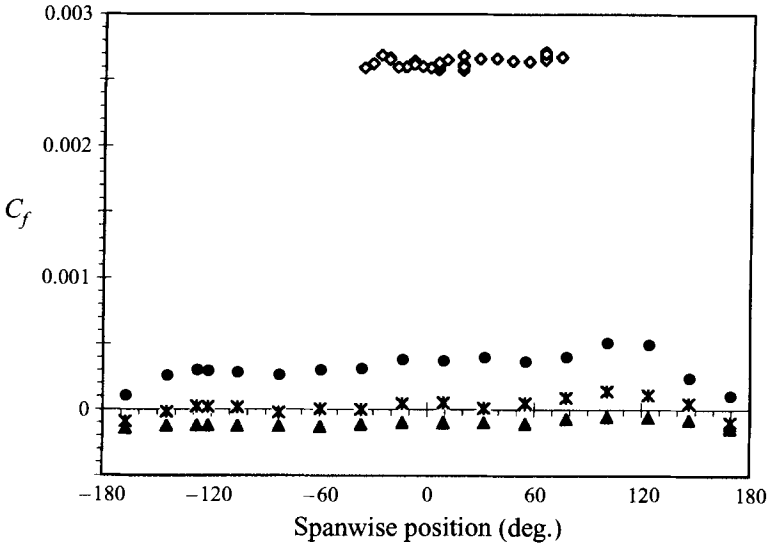

FIGURE 3. Spanwise skin-friction distribution based on local potential velocity extrapolated to wall, at several streamwise locations. Distance given in bubble lengths from reattachment: •, −1.7; *, −1.4; ▲, −0.9; ◇, 4.3.

are reduced in magnitude after reattachment. The largest non-uniformities occur at ±180°, in the wake of the Pitot-static tube at the throat.

3. Mean flow behaviour

Table 1 lists the mean-flow parameters. Figure 2 shows the streamwise distribution of the static pressure coefficient, C_p, the pressure gradient, the skin friction coefficient, C_f, and the probability of reverse flow at the wall, χ_w:

$$C_p(\xi) = \frac{p(\xi) - p_{throat}}{\frac{1}{2}\rho U^2_{throat}}, \tag{2}$$

$$C_f(\xi) = \frac{\overline{\tau_w}(\xi)}{\frac{1}{2}\rho U^2_{pot}(0)}, \tag{3}$$

$$\chi_w(\xi) = \chi(\xi, y)\Big|_{y=0}, \tag{4}$$

where $p(\xi)$ is the wall static pressure, $\overline{\tau_w}(\xi)$ is the mean wall shear stress measured by the wall-mounted pulsed-wire probe, $U_{pot}(0)$ is the local potential velocity extrapolated to the wall (see discussion below), and $\chi(\xi, y)$ is the probability of reverse flow at any point. For completeness, figure 2(*b*) includes the skin friction found from a Clauser chart and also the skin friction (using the pulsed-wire measurement of $\overline{\tau_w}(\xi)$)

FIGURE 2. Streamwise distributions of wall parameters. (*a*) •, Static pressure coefficient referenced to dynamic head at throat; ◇, derivative of static pressure coefficient. (*b*) Skin friction coefficient: △, $C_{f,abs}$ (pulsed-wire measurements referenced to dynamic head at throat); •, C_f (pulsed-wire measurements referenced to local potential velocity extrapolated to wall); ×, Clauser-chart measurements referenced to local potential velocity extrapolated to wall. (*c*) Probability of reverse flow at the wall.

	x (m)	ξ	C_p	$\frac{dC_p}{dx}$ (m^{-1})	$\frac{U_{pot}(0)}{U_{throat}}$	χ_w	C_f Clauser	C_f Pulsed wire	δ_{99} (m)	θ (m)	H	Re_θ
1	0.175	−2.2	0.398	2.18	0.75	0.0	0.00185	0.00249	0.0149	0.0023	1.9	2850
2	0.275	−1.5	0.566	1.34	0.65	9.6	0.00057	0.00065	0.027	0.0046	2.2	4850
3	0.325	−1.2	0.595	0.58	0.61	28.0	0.00031	0.00026	0.034	0.0063	2.4	6850
4	0.425	−0.6	0.623	0.27	0.61	74.0		−0.00025	0.047	0.0076	3.2	7520
5	0.525	0.0	0.656	0.32	0.57	47.0		0.00005	0.051	(0.0078)	(2.4)	(7200)
6	0.625	0.7	0.679	0.19	0.57	7.0	0.00057	0.00080	0.063	0.0113	2.09	10400
7	0.725	1.3	0.688	0.056	0.56	0.2	0.00110	0.00151	0.066	0.0123	1.75	11200
8	0.825	1.9	0.690	0.036	0.56	0.0	0.00160	0.00193	0.074	0.0129	1.55	11700
9	0.925	2.6	0.689	−0.010	0.56	0.0	0.0020	0.0022	0.079	0.0129	1.43	11700
10	1.025	3.2	0.688	−0.024	0.56	0.0	0.0022	0.0024	0.079	0.0127	1.37	11400
11	1.225	4.5	0.686	−0.019	0.55	0.0	0.0025	0.0026	0.090	0.0133	1.30	11900
12	1.475	6.1	0.685	0.000	0.56	0.0	0.0026	0.0027	0.103	0.0148	1.25	13300

TABLE 1. Parameters at each measuring station. The streamwise position, x, is measured from the trip-wire location. The reference Reynolds number, U_{throat}/ν, is 1.62×10^6/m. The uncertainties in C_f, δ_{99}, and θ are at most 5%, except at $\xi = 0.0$ where the entries for θ, H, and Re_θ are estimates.

Definitions: $\xi = \dfrac{x - x_{reatt}}{x_{reatt} - x_{sep}}$ $\quad H = \dfrac{\delta^*}{\theta}$ $\quad Re_\theta = \dfrac{U_{pot}(0)\theta}{\nu}$.

non-dimensionalized by the dynamic pressure at the throat:

$$C_{f,abs}(\xi) = \frac{\overline{\tau_w}(\xi)}{\frac{1}{2}\rho U_{throat}^2}. \tag{5}$$

Mean separation ($\xi = -1$) and reattachment ($\xi = 0$) are defined as the points where $\chi_w = 50\%$ and $C_f = 0$; the figure clearly shows these points to be coincident for both separation and reattachment, as is consistent with other work in two-dimensional separation bubbles (*e.g.* Ruderich & Fernholz 1986). In dimensional units, the mean separation bubble occurs over the region 0.361 m $< x <$ 0.518 m ($\ell = 0.157$ m), where x is measured from the position of the tripping device, located where the nosecone joins the cylindrical test surface.

The separation is caused by an adverse pressure gradient, at its strongest between the throat and separation (figure 2*a*)†; here the skin friction drops sharply. Separation actually occurs near a local minimum in the pressure gradient in this study, and the flow reattaches in a mild adverse pressure gradient. Nonetheless, the wall shear becomes positive and increases downstream of reattachment. It remains low in absolute terms (see $C_{f,abs}$ in figure 2*b*), levelling off to about 0.0008 of the throat dynamic pressure at the far end of the test section. However, by that point the free-stream velocity is also only about half what it was in the throat, so that based on the free-stream dynamic head the far-downstream skin friction recovers to about 0.0027, which is fairly typical for an unperturbed flow at this Reynolds number: Schlichting (1979, equation 21.12) gives $C_f \simeq 0.0025$ at the measured $Re_\theta \simeq 12000$.

The probability of reverse flow is less than 80% throughout the flow. That χ_w is nowhere 100% raises the possibility that the bubble may vanish instantaneously; this, however, seems unlikely without further supporting evidence, particularly given the strong adverse pressure gradient downstream of the throat. Another possibility is

† Various non-dimensionalizations of the pressure gradient are given in AF.

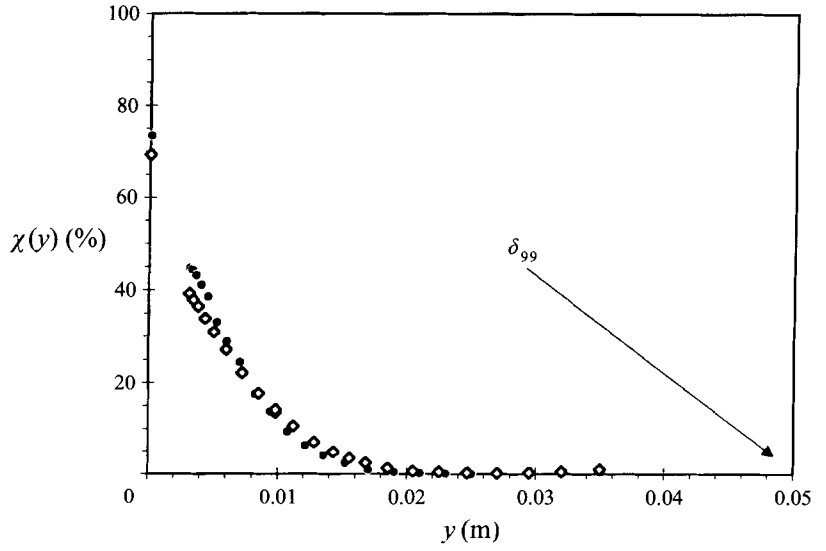

FIGURE 4. Profiles of the probability of reverse flow over the thickest part of the bubble. Distance given in bubble lengths from reattachment: •, −0.6; ◇, −0.3.

that the bubble as a whole is buffeted around in interaction with the boundary-layer flow, moving alternately upstream and downstream by distances of the order of the bubble length so that no one location is always within the bubble. (Note, however, that in the mean sense the bubble location is well defined and quite repeatable from day to day.) Buffeting is consistent with the observation that intermittent reverse flow, $0\% < \chi_w < 50\%$, occurs over about one bubble length upstream and downstream of the region of mean separation, and with the observations of Simpson *et al.* (1981*b*) in an open separation region and by Wagner & Fernholz (see Fernholz 1993) in a strong reverse-flow region.

The separation bubble, in addition to being transient in the sense of the preceding paragraph, is also shallow. Normal profiles of the probability of reverse flow, $\chi(y)$, over the thickest part of the bubble are plotted in figure 4 and show that even for $y = 3.1$ mm (the closest to the wall the traversing pulsed-wire probe measures), χ is always less than 50%. This shows that the mean separation bubble is less than 3 mm high, corresponding to less than 5% of the thickness of the boundary-layer over the bubble. This shallow bubble is similar to Case 3 in DF, except that it occurs much farther upstream in the present study.

The mean velocity profiles are plotted in figure 5 in dimensional units to show the deceleration and thickening of the boundary layer. The figure also shows that the free stream is slightly non-uniform between the nozzle throat and the location of the mean separation bubble ($\xi < 0$), owing to the nozzle divergence and mass removal in that region. The potential-core velocity is well approximated by a straight line whose slope depends on the streamwise position; in this sense, the potential velocity at a given streamwise position, $U_{pot}(y)$, can be extrapolated into the boundary layer and onto the wall to find $U_{pot}(0)$ (see AF for more details). At a given position, $U_{pot}(0)$ is always within 4% of the maximum speed in the boundary layer. These small potential-flow variations in the early profiles are not expected to have a significant effect on the boundary-layer development.

The transition from pulsed-wire to hot-wire measurements is smooth in all profiles

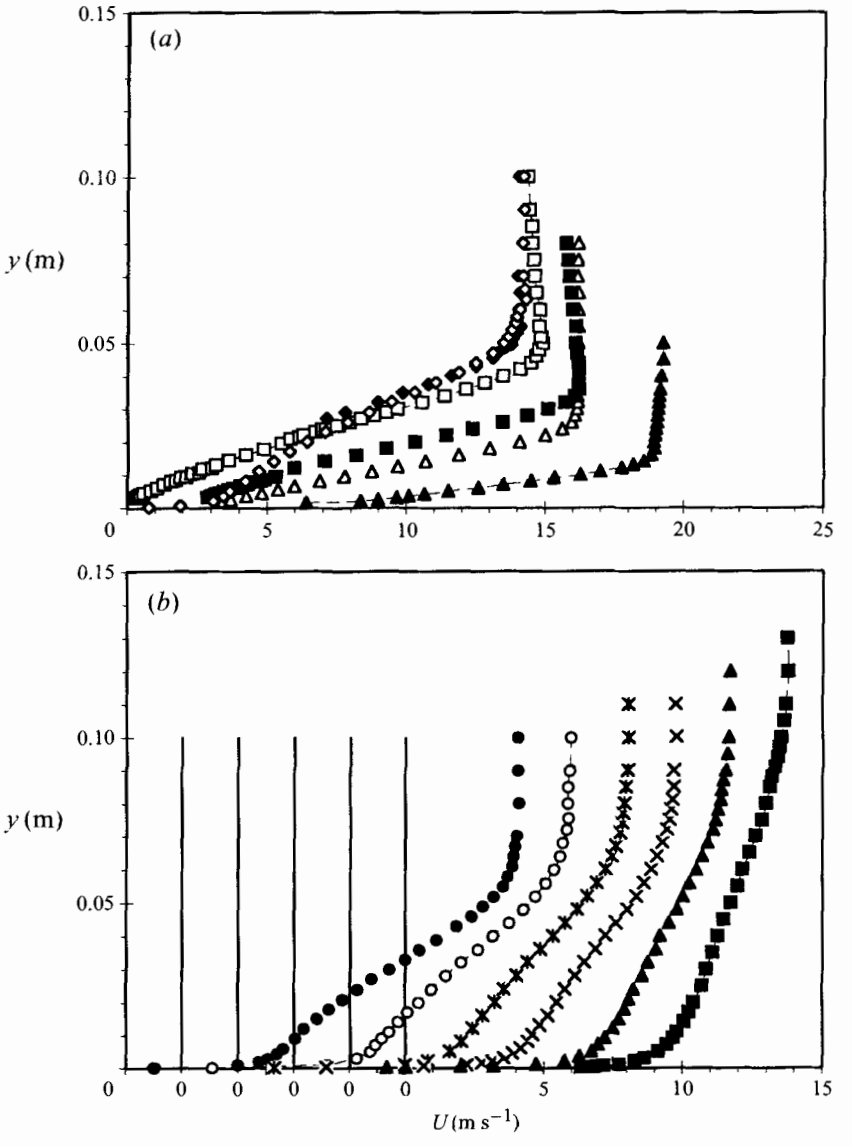

FIGURE 5. Mean-velocity profiles in dimensional coordinates. (*a*) $\xi < 1$. (*b*) $\xi > 1$. (Note the offset on the horizontal axis in *b*.) Symbols: ξ = ▲, −2.2; △, −1.5; ■, −1.2; Box, −0.6; ◆, 0; ◇, 0.7; •, 1.3; ○, 1.9; *, 2.6; ×, 3.2; ▲, 4.5; ■, 6.1.

except one, implying that each technique is valid in the flow regime for which it is used. The notable exception is the profile at reattachment ($\xi = 0$), where the pulsed-wire measurements are in doubt because they do not appear to extrapolate to the zero-wall-shear condition measured by the wall pulsed wire. The pulsed-wire probe provides significantly more blockage at the measuring location than does the hot-wire probe, because the shaft of the former is normal to the test surface directly above the measuring location, while in the latter case the measuring tip is of the order of δ_{99} upstream of the shaft. To test whether blockage affected the pulsed-wire measurements, the blockage was reduced by inserting the pulsed wire from the side

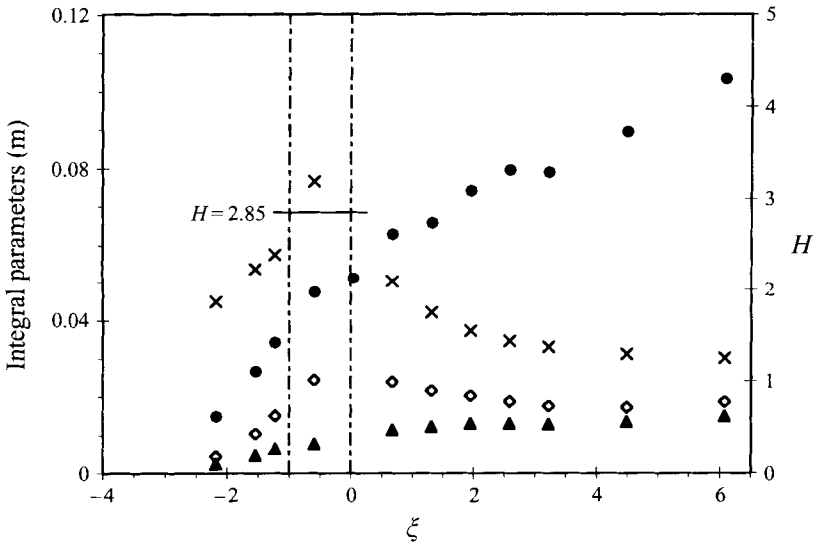

FIGURE 6. Streamwise growth of integral parameters. •, δ_{99}; ◇, δ^*; ▲, θ; ×, $H = \delta^*/\theta$.

instead of from above. The results do not change except at reattachment, where the pulsed-wire and hot-wire results are in closer agreement but still do not match smoothly. For this reason, pulsed-wire measurements at $\xi = 0$ are not presented here. These observations show that reattachment is extremely sensitive to disturbances, in this flow more sensitive even than is separation, which was itself shown by DF to be strongly affected by slight changes in the streamwise pressure gradient. The extra sensitivity at reattachment may be explained in part by the lower mean momentum there.

The integral parameters from these profiles are plotted in figure 6. δ_{99} is found by fitting the velocity profile near the outer edge to an exponential approach to the potential velocity $U_{pot}(y)$ and evaluating the curve fit to find the point $y \equiv \delta_{99}$ such that $\overline{U}(\delta_{99}) = 0.99 U_{pot}(\delta_{99})$. The displacement and momentum thicknesses are defined below in axisymmetric flow for the case in which the potential velocity depends on the distance from the wall:

$$\int_0^{\delta^*} \{U_{pot}(y)\}\{y+R\}\,\mathrm{d}y = \int_0^{\infty} \{U_{pot}(y) - \overline{U}(y)\}\{y+R\}\,\mathrm{d}y, \tag{6}$$

$$\int_0^{\theta} \{U_{pot}^2(y)\}\{y+R\}\,\mathrm{d}y = \int_0^{\infty} \overline{U}(y)\{U_{pot}(y) - \overline{U}(y)\}\{y+R\}\,\mathrm{d}y, \tag{7}$$

where R is the radius of the inner cylinder. (For $\xi > 0$, $U_{pot} \neq U_{pot}(y)$ and the formulae reduce to the analytic expressions given for δ and θ in DF.) The integrations were performed using Simpson's rule for unevenly spaced data. For the profiles in which the log law is valid, the near-wall contributions to the right-hand side were calculated by integrating the universal law instead of $\overline{U}$ up to $y^+ = 50$; for the other profiles, the measured data were used in conjunction with the no-slip condition at the wall. The shape factor H is defined as the ratio of the displacement to momentum thicknesses.

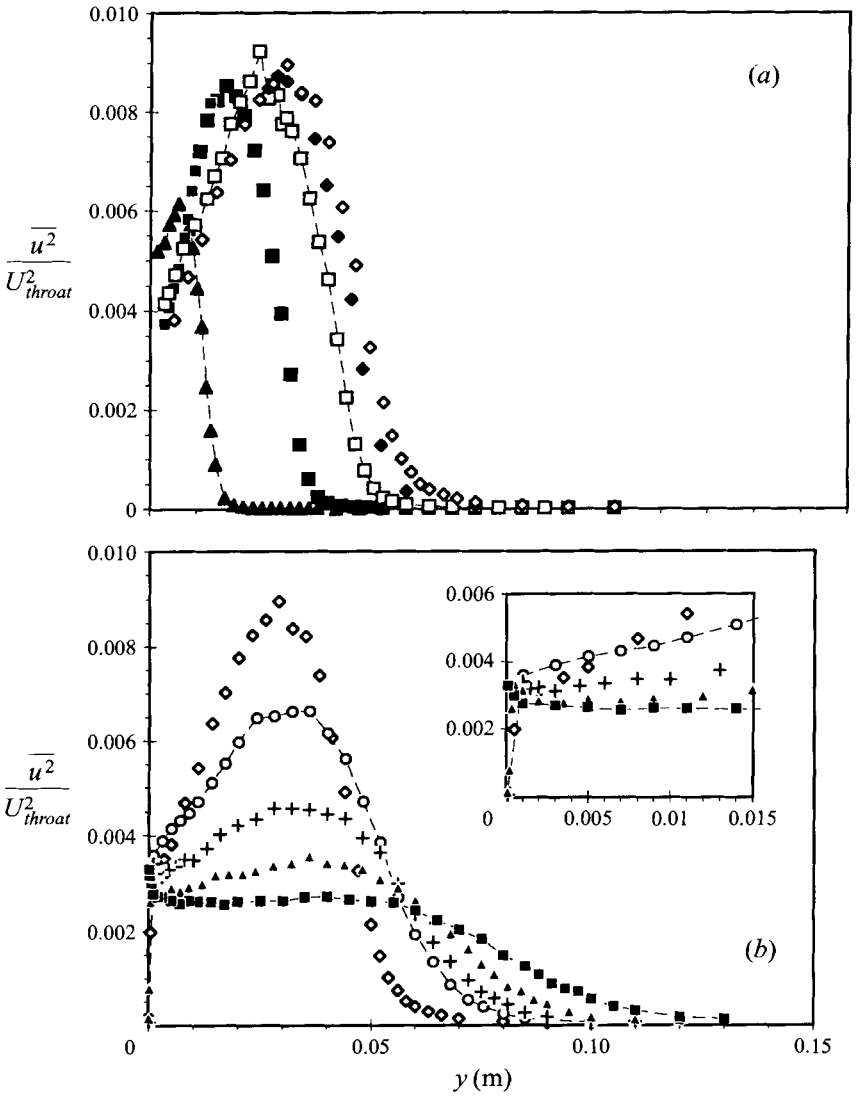

FIGURE 7. Streamwise component of the Reynolds stress: $\overline{u^2}/U^2_{throat}$. (*a*) $\xi \leqslant 0.7$. (*b*) $\xi \geqslant 0.7$. Symbols as in figure 5. Flagged points represent pulsed-wire measurements, while the other data were taken with normal hot wires.

For $\xi > 0$ the increased precision in the listed values of H (table 1) reflects the increased confidence in δ^* after reattachment.

Figure 6 shows that δ_{99} and θ increase monotonically through separation, reattachment, and recovery, whereas the displacement thickness δ^* reaches a shallow local maximum in the separation bubble and falls after reattachment. $\mathrm{d}\delta^*/\mathrm{d}x$ only becomes positive again for $\xi > 4$, where δ^* falls to about the same value as at separation. δ^* is responsible for the sharp increase in the shape factor over the bubble, which is characteristic of a separating boundary layer and which vanishes at reattachment. DF point out this is why inverse methods, in which δ^* is an input to the calculation, give good results for separating flows. DF found that $H = 2.85 \pm 0.1$ is characteristic at separation for flows of this type and this is consistent with both separation and

reattachment in the present work. The behaviour of H is similar to that seen by Moses (1964) and Goldberg (1966) in early works on axisymmetric turbulent boundary layers subjected to APG. In each work (Moses Case 3, and Goldberg Case 5) a turbulent boundary layer is decelerated – possibly to separation – and then allowed to relax in almost ZPG. Similar peaks in H are seen around the ends of the APG regions (Goldberg shows that this corresponds to the minimum estimate of C_f as measured with sub-layer fences and Preston tubes). In both works the return to ZPG brings a decrease in H, as is consistent with the present work. Instrumentation limitations at the time prevented those workers from measuring accurately in the region of reverse flow or even quantifying the degree of reverse flow, so it is impossible to make more exact comparisons to relate the behaviour of H to χ.

The scaling of the mean velocity profile is discussed in the companion paper AF. The most important results are summarized here. The profile proposed by DF as universal for turbulent boundary layers close to separation was found to agree well with the data in the range $-1.5 \leqslant \xi \leqslant 1.3$, which includes two profiles after reattachment. This is in spite of the different pressure-gradient histories in these flows. This profile uses Perry–Schofield (1973) scaling for non-dimensionalizing the velocity and distance from the wall, but it does not relate the speed scale, u_s, to Reynolds-stress levels as the original authors do. DF proposed, instead, that both u_s and H depend only on χ_w in this sort of flow, and the results in AF show good agreement with the proposed relationships even in the reattaching flow. This reinforces the importance of the amount of reverse flow at the wall. Downstream of the separated region, the universal log law becomes valid again about 3 bubble lengths after reattachment. The wake region, on the other hand, remains distorted even at the measuring station farthest downstream. There, the wake factor is smaller than expected in ZPG flows, and it is inferred this indicates weaker outer-layer structures than in the canonical case.

4. Turbulence measurements

Profiles of the Reynolds stresses are plotted in figures 7–10 with the distance normal to the wall, y, given in dimensional units to show the growth of the boundary layer and the absolute positions of the stress peaks. The axisymmetric form of the transport equation for turbulence kinetic energy is

$$\begin{aligned}\frac{\mathrm{D}}{\mathrm{D}t}\left(\frac{\overline{q^2}}{2}\right) = &-\frac{1}{\rho}\frac{\partial}{\partial x}\left(\overline{p'u}\right) - \frac{1}{\rho r}\frac{\partial}{\partial y}\left(\overline{rp'v}\right) - \frac{1}{r}\frac{\partial}{\partial y}\left(r\overline{\frac{vq^2}{2}}\right) - \frac{\partial}{\partial x}\left(\overline{\frac{uq^2}{2}}\right)\\ &+ (-\overline{uv})\frac{\partial \overline{U}}{\partial y} + \left(\overline{u^2} - \overline{v^2}\right)\frac{\partial \overline{V}}{\partial y} + \left(\overline{u^2} - \overline{w^2}\right)\frac{\overline{V}}{r}\\ &+ \frac{\nu}{r}\frac{\partial}{\partial y}\left(r\frac{\partial}{\partial y}\frac{\overline{q^2}}{2}\right) + \nu\frac{\partial^2}{\partial x^2}\left(\frac{\overline{q^2}}{2}\right) - \frac{\nu}{r^2}\left(\overline{v^2} + \overline{w^2}\right) + \text{viscous dissipation},\end{aligned} \tag{8}$$

where $r = y + R$ and R is the radius of the inner cylinder. Figure 11 shows the production and turbulence-transport terms of equation (8). Terms in the transport of $-\overline{uv}$ are not shown, but they are similar to those shown for $\frac{1}{2}\overline{q^2}$. Terms due solely to the transverse curvature, in which $1/r$ appears without any spatial derivative, are in the present investigation typically at least an order of magnitude smaller than the largest terms in the above equation, so the presence of transverse curvature in this

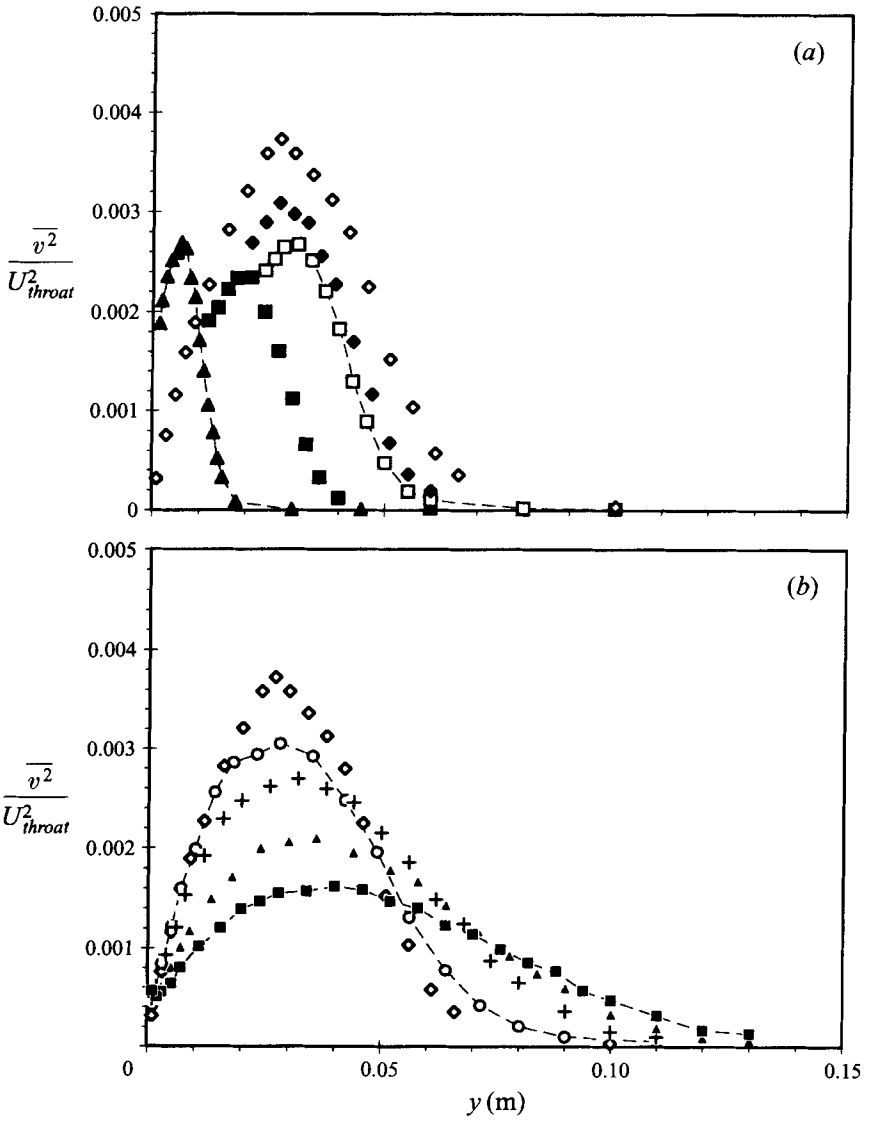

FIGURE 8. Wall-normal component of the Reynolds stress: $\overline{v^2}/U^2_{throat}$. (*a*) $\xi \leqslant 0.7$. (*b*) $\xi \geqslant 0.7$. Symbols as in figure 5.

study does not introduce substantially new dynamical effects not present in the flow along a planar surface. First we briefly discuss the flow until the end of separation to prove that it is typical and to address a few open issues in this field, and then we move on to discuss the relaxation behaviour after reattachment.

For the profiles until the end of separation ($\xi < 0$), the behaviour is characteristic of that seen in other APG studies in spite of the early APG imposed on this flow. The mean shear $\partial U/\partial y$ decreases near the wall and increases away from the wall. This results in a shift in both the production peak (figure 11*a*) and the Reynolds-stress peaks (figures 7*a*–10*a*) to roughly the middle of the boundary layer. Turbulence transport (figure 11*b*) functions in its usual manner to redistribute these stress peaks towards the outer edge of the boundary layer.

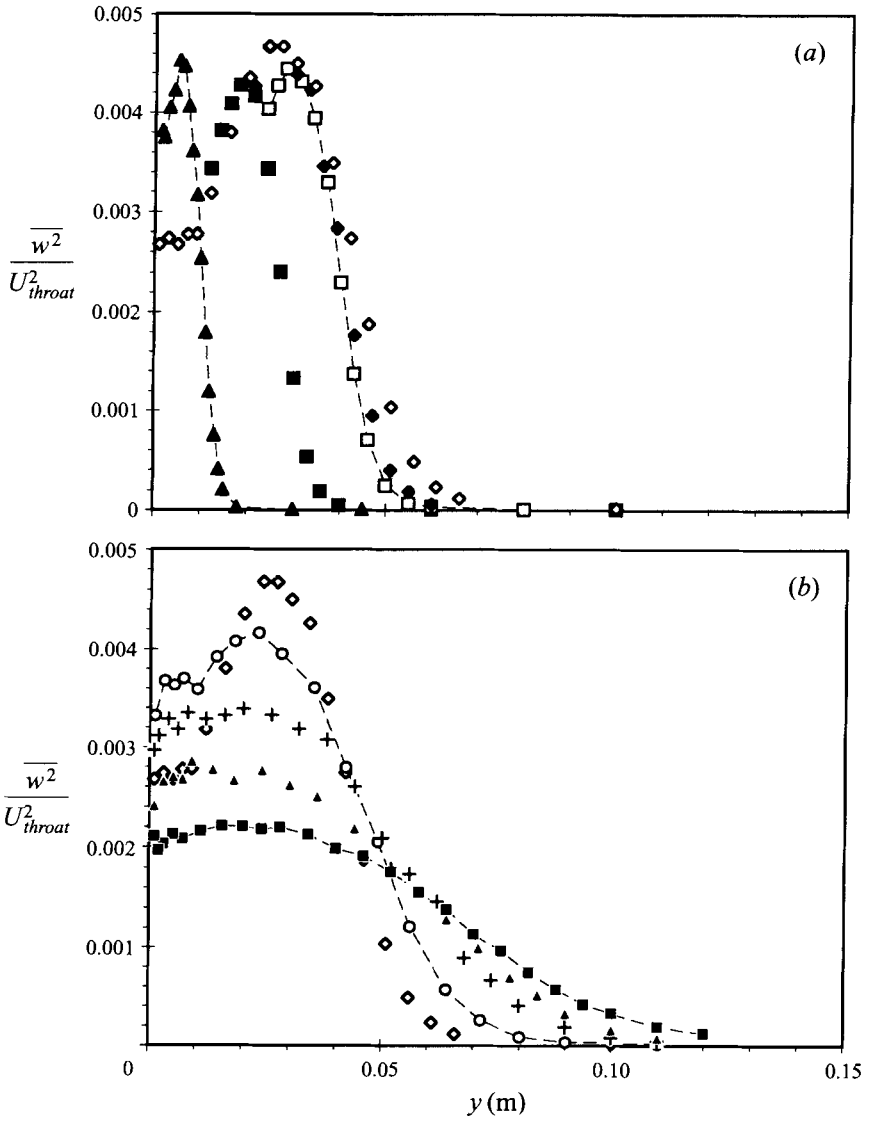

FIGURE 9. Spanwise component of the Reynolds stress: $\overline{w^2}/U^2_{throat}$. (*a*) $\xi \leqslant 0.7$. (*b*) $\xi \geqslant 0.7$. Symbols as in figure 5.

To provide a global view of the stress behaviours, we plot in figure 12(*a*) the net streamwise flux of turbulence kinetic energy integrated across the boundary layer and in figure 12(*b*) the integrated flux of production. To the end of separation ($\xi < 0$) the flux of $\frac{1}{2}\overline{q^2}$ increases while the flux of its production decreases. This suggests the role of dissipation lessens around the separation bubble, which is consistent with Robinson's (1991*b*) ZPG results showing dissipation is caused by stretching due to the mean shear. Driver (1991) drew a similar conclusion.

Interestingly, while the flux of $-\overline{uv}$ follows a similar pattern to the flux of $\frac{1}{2}\overline{q^2}$ (figure 12*a*), the behaviours of their production fluxes are quite different (figure 12*b*), with the net production of $-\overline{uv}$ increasing by about 35% over the bubble. This is double the uncertainties in the $-\overline{uv}$ integrals over the bubble (15–20%); furthermore,

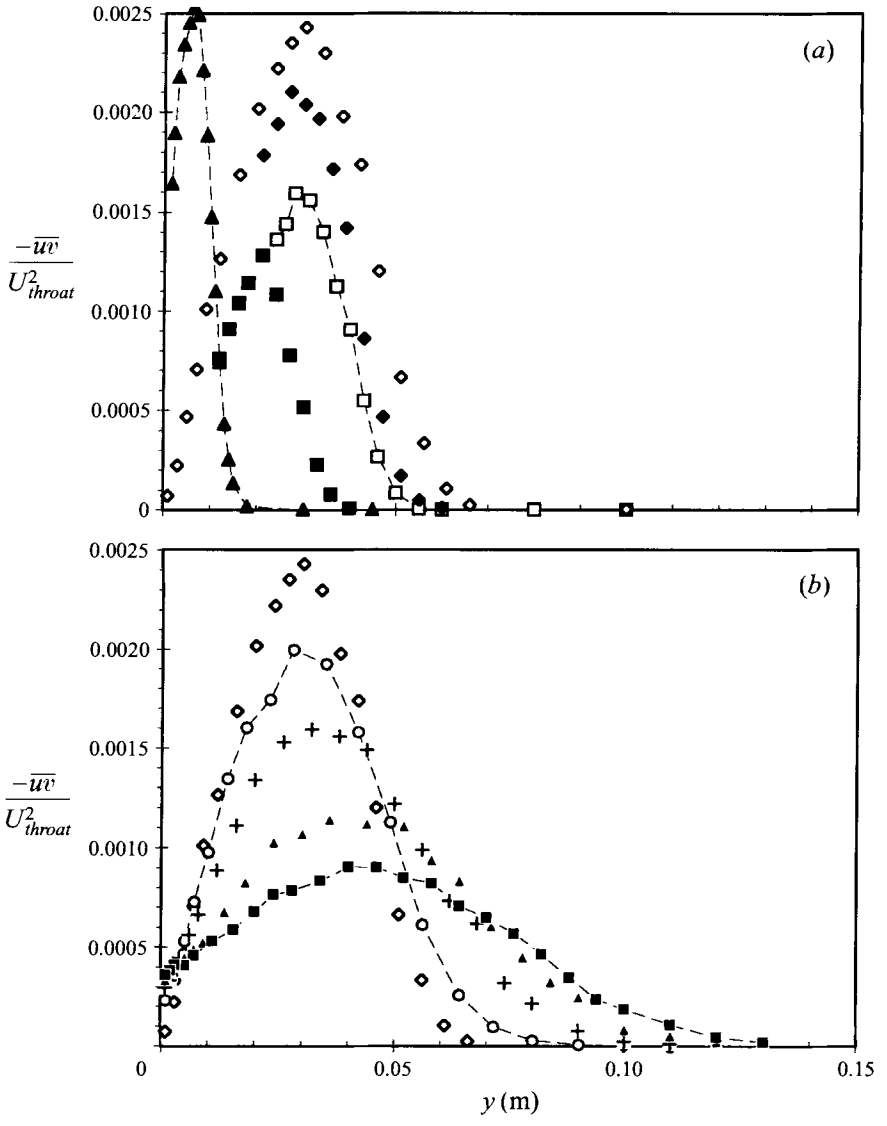

FIGURE 10. Shear component of the Reynolds stress: $-\overline{uv}/U^2_{throat}$. (*a*) $\xi \leqslant 0.7$. (*b*) $\xi \geqslant 0.7$. Symbols as in figure 5.

in the relaxation region the uncertainties are reduced by about half and the separation remains between the two sets of data in figure 12(*b*). Thus, the divergence seen in figure 12(*b*) implies a new mechanism for shear-stress production over the bubble which is decoupled from the production of turbulence kinetic energy. One mechanism which would be absent in ZPG flows but which has been observed in other separating flows is the vertical oscillation of the shear layer as lumps of fluid move between the shear layer and the reverse-flow region. This has been seen by Simpson *et al.* (1981*b*) in strong, open-bubble separations, but it is not known whether such behaviour occurs in a mild, closed-bubble separation like this one. If the differing production behaviours is, in fact, indicative of such oscillations, it must be recognized that the

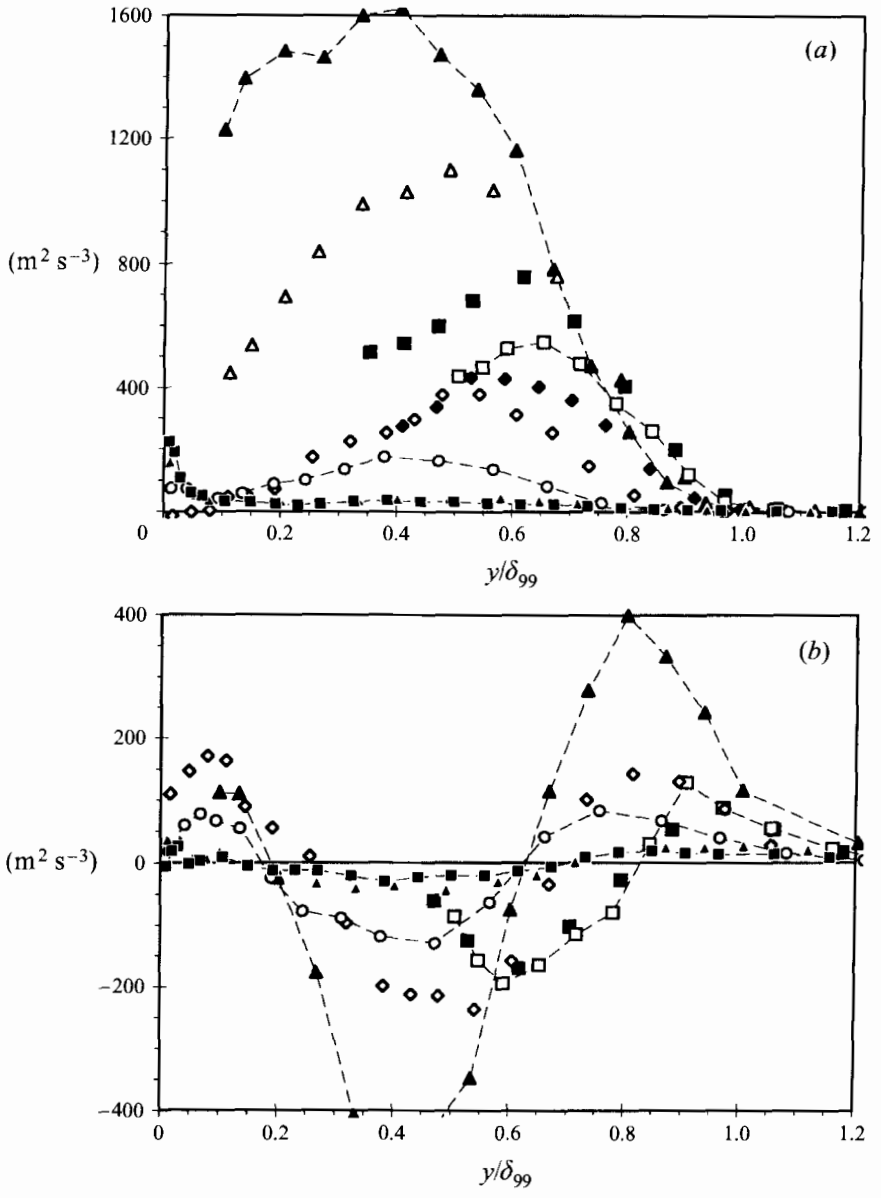

FIGURE 11. Terms in the transport equation for turbulence kinetic energy. (*a*) Production $(-\overline{uv})\,\partial\overline{U}/\partial y + (\overline{u^2} - \overline{v^2})\,\partial\overline{V}/\partial y + (\overline{u^2} - \overline{w^2})\,\overline{V}/r$. (*b*) Normal transport $(1/r)(\partial/\partial y)\left(r\overline{\tfrac{1}{2}vq^2}\right)$. Symbols as in figure 5.

spectral data (not shown) prove they are not periodic, as is the case in some strongly separated flows (e.g. Cherry, Hillier & Latour 1984).

Another issue of interest in separating flows is the role of the normal-stress terms in the production of turbulence (see equation (8)). Simpson *et al.* (1981*b*) showed they are significant in open-bubble flows, but DF found them insignificant in their mild, closed-bubbles similar to the one studied here. For the present work, figure 13 shows the ratio of the normal-stress terms to the shear-stress term in the production

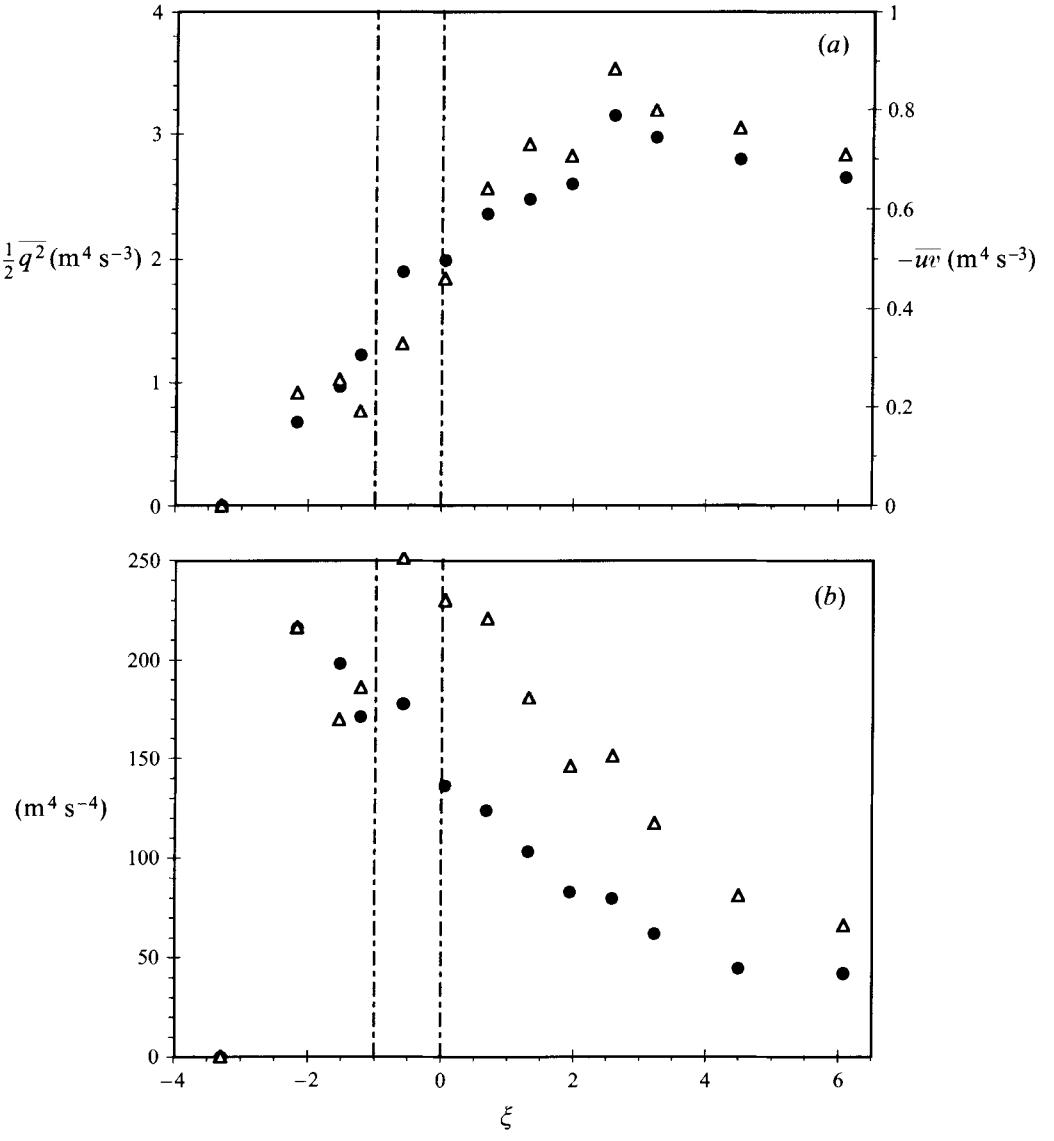

FIGURE 12. Streamwise flux integrated across the boundary layer $(1/R)\int_0^{\delta_{99}} < > \overline{U}r\mathrm{d}y$. (*a*) Flux of Reynolds stresses. (*b*) Flux of production. Symbols: •, $\frac{1}{2}\overline{q^2}$; △, $-\overline{uv}$.

of $\frac{1}{2}\overline{q^2}$. At the most upstream profile the normal-stress terms are small as is typical of ZPG flows, but they increase in importance near the separation bubble. At $\xi = -1.2$, they are 75% as large as the shear-stress term in the outer half of the boundary layer. The reason for the difference from DF is that in their work the flow was carefully tailored to remain on the verge of separation for a finite length, so

$$\frac{\partial \overline{U}}{\partial x} = -\frac{1}{r}\frac{\partial (r\overline{V})}{\partial y} \simeq 0.$$

The present results show that the normal-stress terms cannot necessarily be neglected

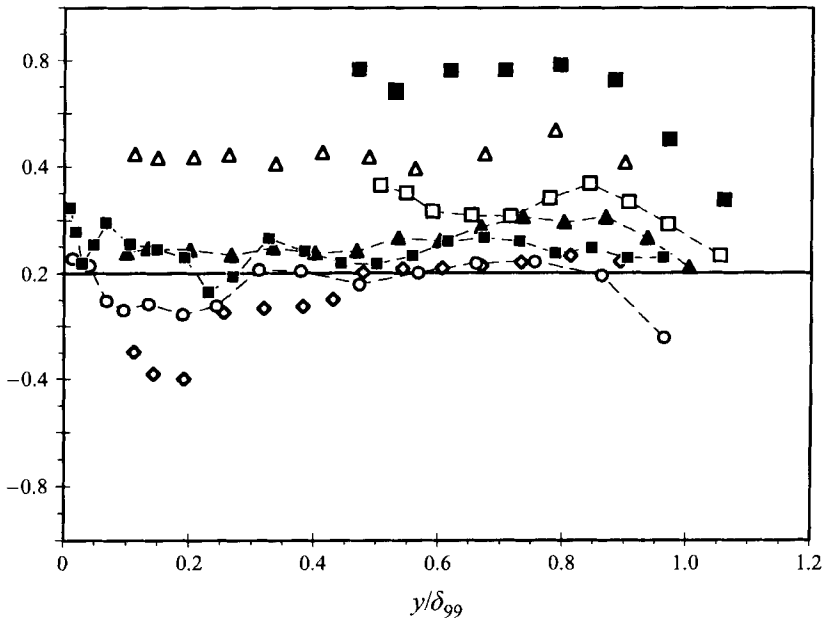

FIGURE 13. Contributions to production of turbulence kinetic energy: ratio of normal-stress to shear-stress terms, $\left[\left(\overline{u^2}-\overline{v^2}\right)\partial\overline{V}/\partial y+\left(\overline{u^2}-\overline{w^2}\right)\overline{V}/r\right]/(-\overline{uv})\,\partial\overline{U}/\partial y$. Symbols as in figure 5.

even in such a mild separation. Another small difference from the DF results is that they found a small plateau in the $\overline{u^2}$ profile near the wall only in the case of mean reverse flow ($\chi > 50\%$) and not in the cases where χ was everywhere less than 50%. They suggested that the plateau was characteristic of mean reverse flow, but the present results do not support this statement.

Next, we consider the behaviour of the flow field as the boundary layer reattaches ($\xi = 0$) and relaxes in nominally ZPG. We showed that over the separation bubble the behaviour is quite typical of separated flows despite it upstream history. Not only do the stress profiles have the characteristic peaked shapes, but the magnitudes and positions of the peaks are in fact quite comparable to those found by DF in boundary layers which grew in ZPG before being brought to separation (see their figures 10 and 11). Therefore, the general character of the relaxation behaviour shown here is not expected to be overly dependent on the details of the pre-separation history.

After reattachment, the Reynolds-stress behaviour is shown in figures 7(*b*)–10(*b*). In the outer part of the boundary layer (say, $y > 0.03$ m), all components of the Reynolds stresses relax in the same manner: the stress peaks drop and the stress levels grow near the edge of the boundary layer, in part due to redistribution by turbulence transport (figure 11*b*). The peak in production (figure 11*a*) and the minimum in turbulence transport (figure 11*b*) continue to track with the peaks in the Reynolds-stress profiles, although their magnitudes decrease uniformly throughout the relaxation region, as do the integrated production fluxes (figure 12*b*). The normal stresses play no significant role in production (figure 13).

Closer to the wall ($y < 0.03$ m) the Reynolds stress behaviour varies by component. The spanwise ($\overline{w^2}$) component responds first, forming a plateau near the wall (figure 9*b*). Although the near-wall crossed-wire measurements at $\xi = 0.7$ are uncertain, this trend is more pronounced at $\xi = 1.9$ and $\xi = 3.2$, where measurements are easier to

make. The other profiles are not nearly so flat at these positions. This behaviour can be explained in terms of inviscid vortex dynamics. As the shear layer reattaches, the flow speeds up near the wall ($\partial\overline{U}/\partial x > 0$) and the mean shear $\partial\overline{U}/\partial y$ increases. Both of these factors increase the streamwise vorticity through the inviscid tilting/stretching mechanism, as seen from the instantaneous vorticity-transport equation:

$$\frac{\mathrm{D}\omega_x}{\mathrm{D}t} = \omega_x \frac{\partial U}{\partial x} + \omega_y \frac{\partial U}{\partial y}. \tag{9}$$

Tilting rotates ω_y into ω_x, converting ($\overline{u^2}$ and $\overline{w^2}$) to ($\overline{v^2}$ and $\overline{w^2}$), giving a net gain of $\overline{v^2}$ at the expense of $\overline{u^2}$. Stretching increases the strength of ω_x, increasing $\overline{v^2}$ and $\overline{w^2}$. The impermeability boundary condition requires the addition of image streamwise vorticity of equal and opposite strength, causing the v fluctuations to cancel and the w fluctuations to increase in the region near the wall. The overall effect is most strongly to increase $\overline{w^2}$ near the wall with little influence on $\overline{v^2}$, as observed in figures 9(*b*) and 8(*b*). Although this mechanism predicts a simultaneous decrease in $\overline{u^2}$ figure 7(*b*) shows that this stress is little altered near the wall, due to the combination of production, dissipation, and transport into that region (figure 11). This argument interprets a change of the instantaneous vorticity in terms of its effect on the Reynolds-averaged stresses, something of a mixed metaphor. An analysis of the Reynolds-averaged vorticity-transport equation is beyond the scope of this paper, but we believe this argument offers insight into the way that the near-wall $\overline{w^2}$ behaviour differs markedly from that of the rest of the Reynolds stresses. Also, note that this discussion assumes the presence of instantaneous vorticity in the inner region, but not necessarily vorticity organized into 'vortex' structures.

The $\overline{u^2}$ profiles (figure 7*b*) do not show the same early plateau in the inner part of the layer as the $\overline{w^2}$ profiles, but by the last measuring station the stress peak has reduced enough so that the profile is flat over most of the profile. Very close to the wall ($y \lesssim 0.002$ m) there is evidence of a small $\overline{u^2}$ peak and figure 11(*a*) shows a similar near-wall production peak. Both of these are characteristic inner-layer features in ZPG. This regeneration of the near-wall production causes the net flux of production to level off after falling monotonically from upstream (figure 12*b*). Around the same position (say, $\xi \simeq 3$) the fluxes of Reynolds stresses also flatten out after increasing monotonically from upstream. These opposing trends imply that the role of dissipation becomes significant again after this point, which is also the position where the skin friction levels off at a value typical of a boundary layer at its Re_θ (figure 2*b*). These results show that the viscous (no-slip) boundary condition regains its importance in this flow about 3 bubble lengths after reattachment.

The behaviour of the $\overline{v^2}$ (figure 8*b*) and $-\overline{uv}$ (figure 10*b*) stresses in the inner 0.03 m is different from that of $\overline{u^2}$ and $\overline{w^2}$. They never reach a plateau, and in fact they are little changed throughout the relaxation region for $y < 0.03$ m, except that the profile peaks decay in the outer region with boundary-layer thickening. The endurance downstream of reattachment of abnormally small $-\overline{uv}$ levels near the wall is further emphasized in figure 14 showing the 'structure' parameter a_1, the ratio of the shear stress to the sum of the normal stresses. Approaching separation, a_1 drops across the boundary layer in a typical manner (see, for instance, DF). After reattachment, a_1 quickly rises to a level characteristic of boundary layers ($\sim$0.15) in the outer part of the layer. In the inner half of the boundary layer, however, it remains small throughout the relaxation, and this is distinctly different from the canonical case, where a_1 is approximately constant for $y/\delta_{99} > 0.1$. Only in the latter half of the

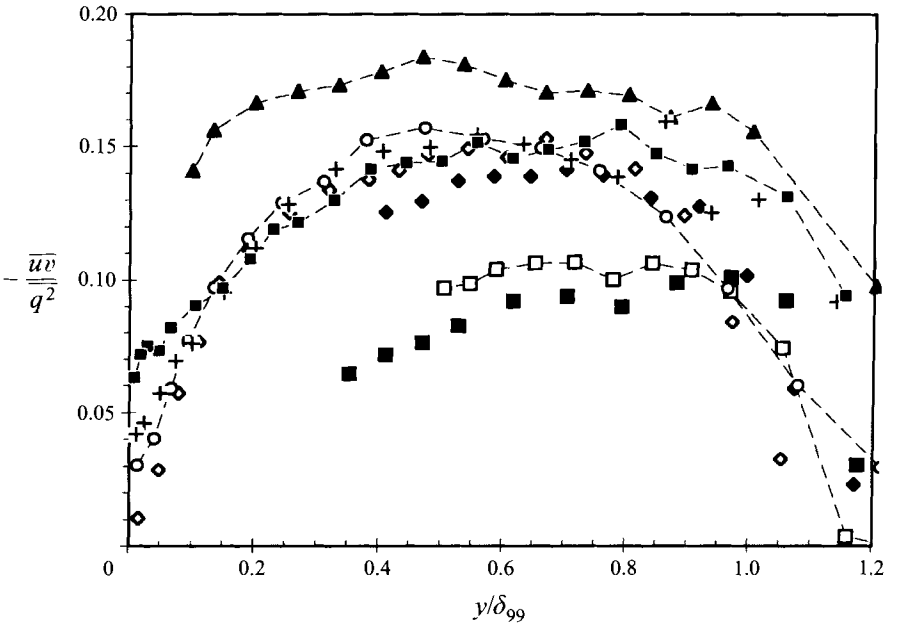

FIGURE 14. Structure-parameter profiles, $a_1 = -\overline{uv}/\overline{q^2}$. Symbols as in figure 5.

recovery length ($\xi > 3$, where viscous effects become important) does the slope near the wall start to increase gradually. The slow response of the Reynolds shear near the wall is an unusual and important feature of this flow and is discussed further in §5.

The moments of the fluctuating skin friction are shown in figure 15; note that these are actually measurements of the streamwise velocity component very close to the wall:

$$\tau_{w,rms}(\xi) = \left(\overline{\tau_w'^2}\right)^{1/2}, \tag{10}$$

$$\tau_{w,inten}(\xi) = \frac{\left(\overline{\tau_w'^2}\right)^{1/2}}{|\overline{\tau_w}|}, \tag{11}$$

$$S_w(\xi) = \frac{\overline{\tau_w'^3}}{\left(\overline{\tau_w'^2}\right)^{3/2}}, \tag{12}$$

$$F_w(\xi) = \frac{\overline{\tau_w'^4}}{\left(\overline{\tau_w'^2}\right)^2}. \tag{13}$$

With the onset of instantaneous reverse flow ($\chi_w > 0$) near $\xi = -2$, the skewness at the wall begins to decrease from its maximum value of about +1.5 and changes sign at separation. This sign change was also observed by DF. Here, we see that the skewness changes sign again at reattachment and peaks where χ_w goes to zero, after which the skewness falls gradually to a final value of 1.4 at $\xi = 6.1$. The observation that the skewness vanishes both at separation and at reattachment can be understood by considering the cause of non-zero skewness in the ZPG boundary layer. There, the positive skewness is attributed to energetic ('sweep') events bringing

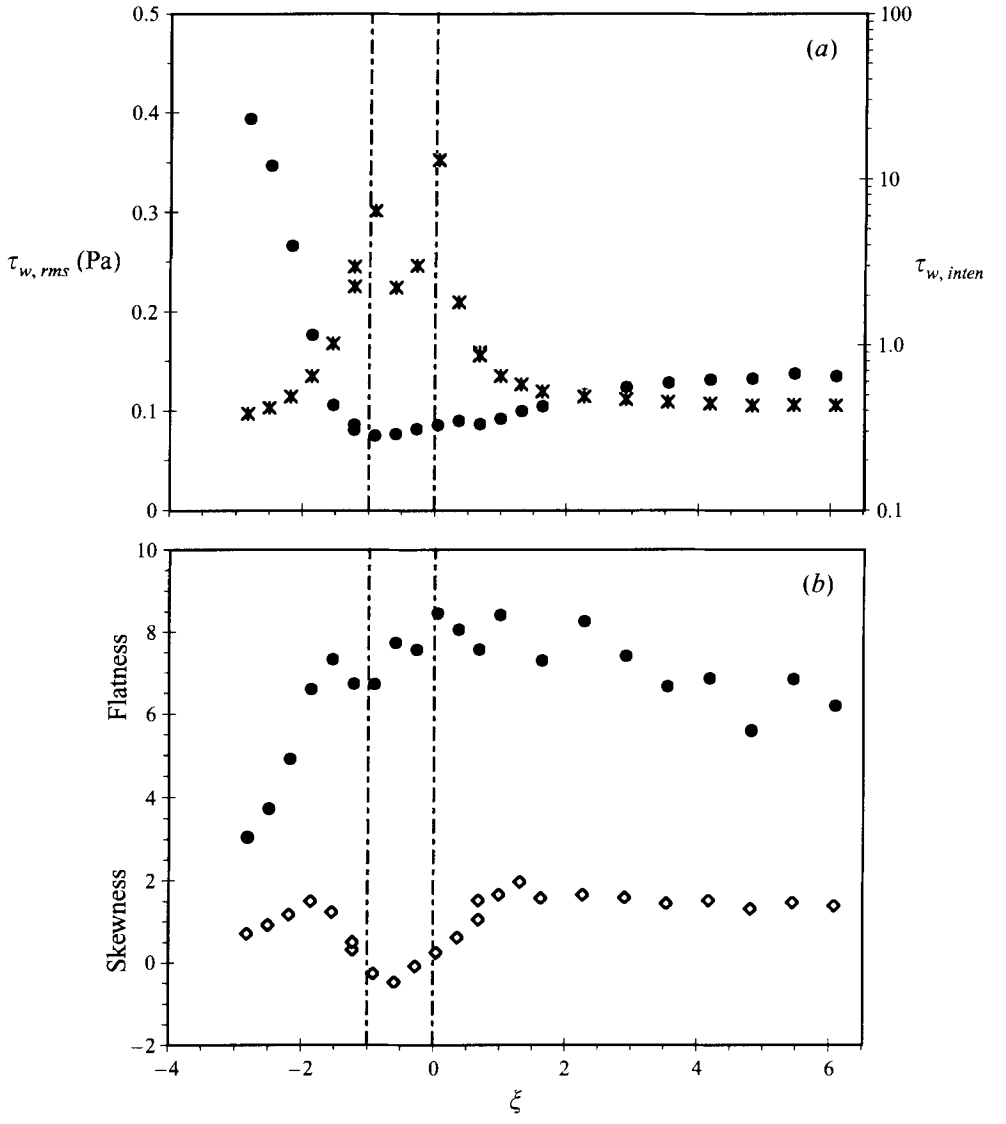

FIGURE 15. Moments of the fluctuating skin friction $C_f'(t)$. (*a*) Second moments: •, $\tau_{w,rms}$; ×, $\tau_{w,inten}$. (*b*) Third moment S_w, ◇; and fourth moment F_w, •.

higher-momentum fluid to the wall (see, for example, Johansson & Alfredsson 1982). The present results extend this description to reverse flow: the sign of the wall skewness corresponds to the sign of the mean-velocity gradient at the wall. For mean reverse flow, energetic perturbations imposed by the fluid approaching the wall are more likely to be in the reverse-flow direction. Where the mean flow is zero away from the wall (at separation and reattachment, $\chi_w = 50\%$), the wallward motions impose no preferred type of perturbation and the wall skewness is zero.

The magnitude or sign of the skewness does not imply anything about the *amount* of activity, since the skewness is an odd moment and can vanish even in the presence of high turbulence. The r.m.s. of the fluctuating skin friction shows that the amount of turbulence at the wall decreases through separation, plateaus under the bubble,

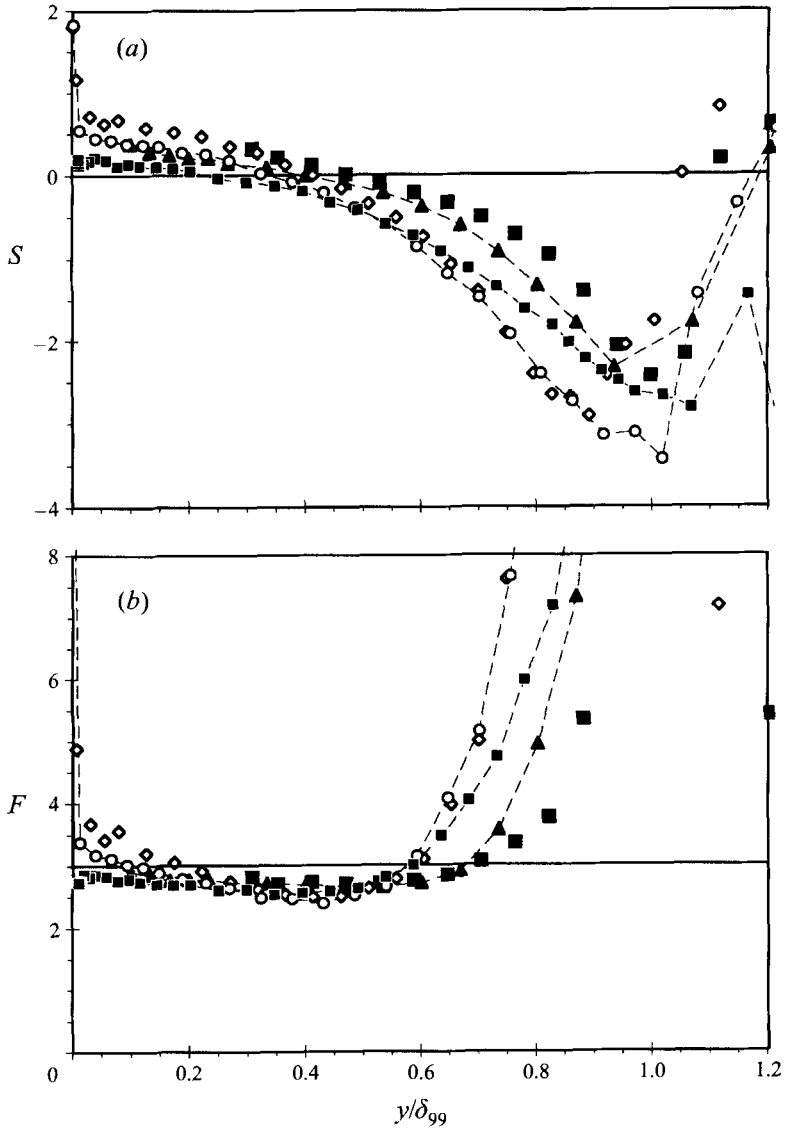

FIGURE 16. Profiles of moments of the streamwise velocity fluctuations $u(t)$.
(*a*) Third moment $\overline{u^3}/\left(\overline{u^2}\right)^{3/2}$. (*b*) Fourth moment $\overline{u^4}/\left(\overline{u^2}\right)^2$. Symbols as in figure 5.

and increases slowly after reattachment. The flatness factor provides information about the *nature* of these wall fluctuations. A large F_w implies the intermittent mixing of turbulent and quiescent fluid; near the wall this is typically attributed to the impingement onto the viscous, near-wall fluid of higher-speed fluid originating away from the wall – such 'sweep' motions presumably being caused by organized motions in the inner and/or outer layers. In the present work, the wall flatness factor increases with the onset of reverse flow and remains high throughout the relaxation region. The enduring high level of F_w suggests that the interaction of the inner/outer layers with the wall fluid continues throughout separation in spite of the decreased turbulent

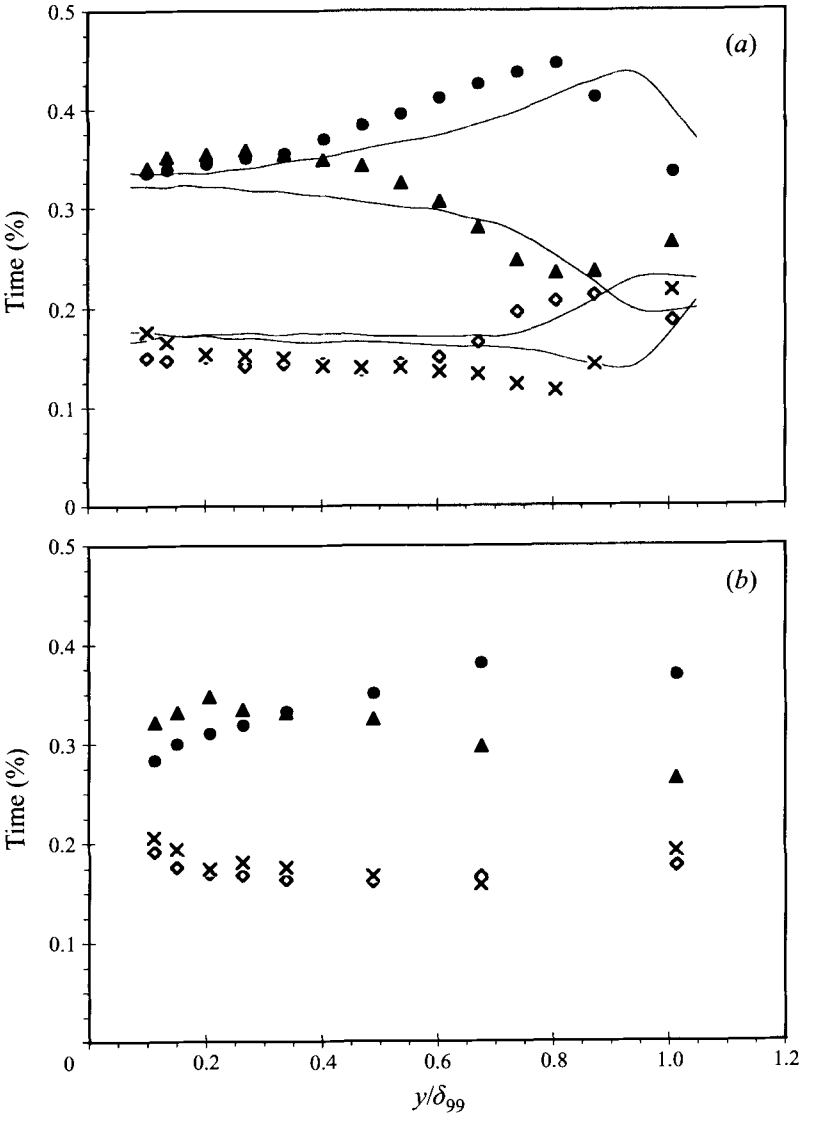

FIGURE 17(*a,b*). For caption see facing page.

activity, and that this interaction, as a fraction of the local turbulence level, becomes *more* important as the turbulence level decreases through separation.

The profiles of the skewness and flatness distributions across the boundary layer (figure 16) show only a little effect of the pressure gradient or separation/reattachment. Small changes in the profiles occur in the outer half of the layer after reattachment, where the skewness becomes more negative and the flatness larger. In an unperturbed boundary layer, a high flatness and a negative skewness near the outer edge are associated with the entrainment of free-stream fluid, resulting in an intermittently turbulent signal. That $F(y)$ and $S(y)$ become larger, at a given y/δ_{99}, after reattachment implies that free-stream fluid is entrained more deeply into the boundary layer,

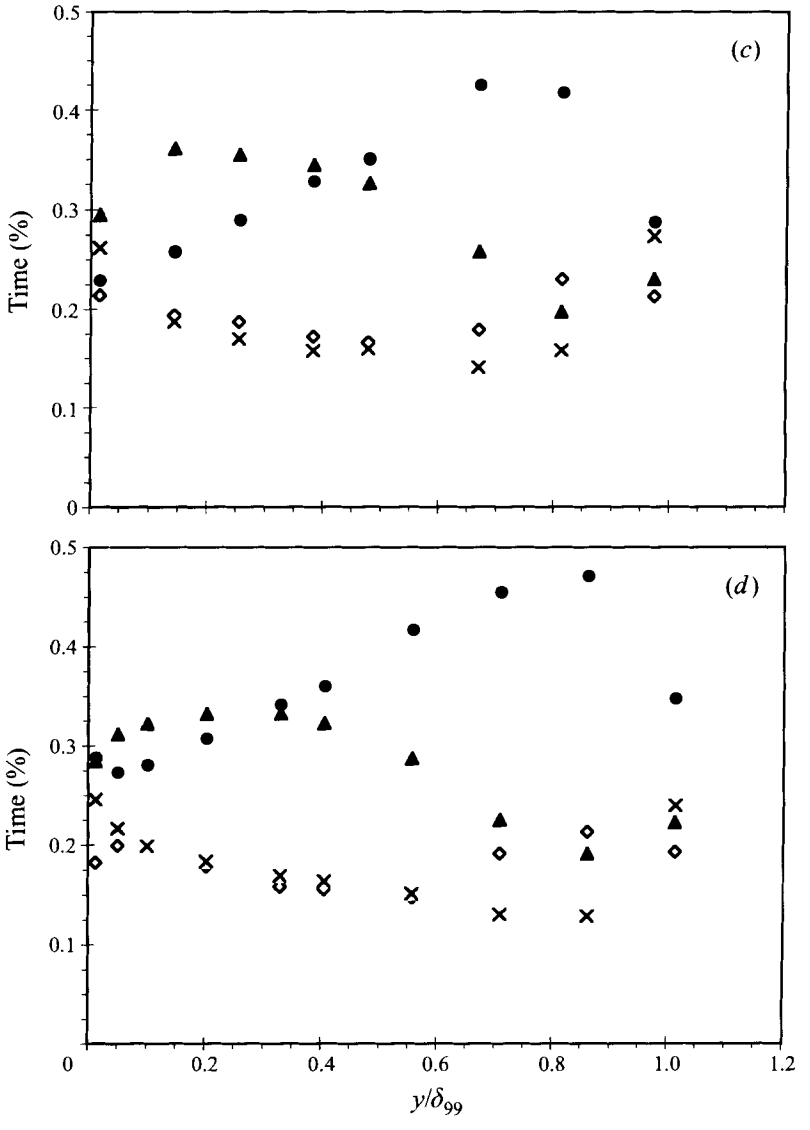

FIGURE 17. Fractional residence time of velocity fluctuations $(u(t), v(t))$ in each quadrant, at several streamwise locations. Upstream of separation: (*a*) $\xi = -2.2$, (*b*) $\xi = -1.5$. After reattachment: (*c*) $\xi = 0.7$, (*d*) $\xi = 3.2$. Symbols: ◇, first quadrant; ▲, second quadrant; ×, third quadrant; •, fourth quadrant. Solid lines typical of unperturbed boundary layer, from Alving (1988).

which again suggests that the large-scale, outer-layer structure remains active and is not killed off by the separation/reattachment process.

Finally, a quadrant decomposition of the fluctuating streamwise and normal velocity components is presented in figures 17 and 18 by quadrant, showing the fractional residence time and the fractional contribution to $-\overline{uv}$, respectively. The solid lines show quadrant contributions typical in an unperturbed layer (Alving 1988). There, Q2 and Q4 events are about equally (35%) likely in the inner layer and contribute 60–70% each to $-\overline{uv}$. Towards the outer edge, Q2 events are less frequent (about 20% at $0.9\delta_{99}$) but more important in the total shear (almost 100% at $0.9\delta_{99}$); Q4

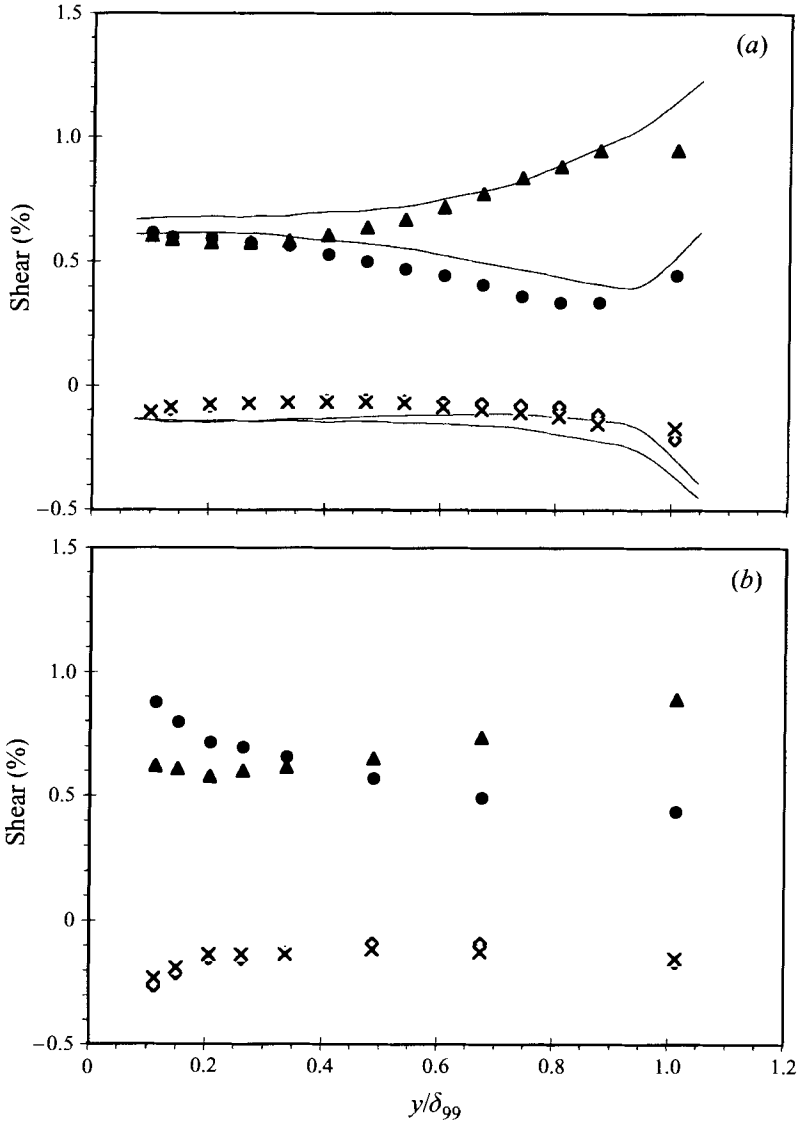

FIGURE 18(*a,b*). For caption see facing page.

events are more frequent and contribute less to $-\overline{uv}$. Upstream of separation, these ZPG trends are well followed by the data in the incoming profile. The striking result is that around separation and after reattachment the trend described above is qualitatively unaffected in the outer layer but becomes reversed in the inner region, so that profiles of Q2 and Q4 cross in both figures: in the inner half of the layer, inflow events are less frequent but more important to the shear stress. Only by the last measuring station does this trend seem to be disappearing, and those profiles (not shown) are very similar to the one at $\xi = -2.2$. Thus, inflow events near the wall are more important in the relaxing boundary layer than in the unperturbed one. This is consistent with the wall flatness factor being large throughout the recovery region, an observation which was attributed to wall sweeps (Q4) caused by the vortex

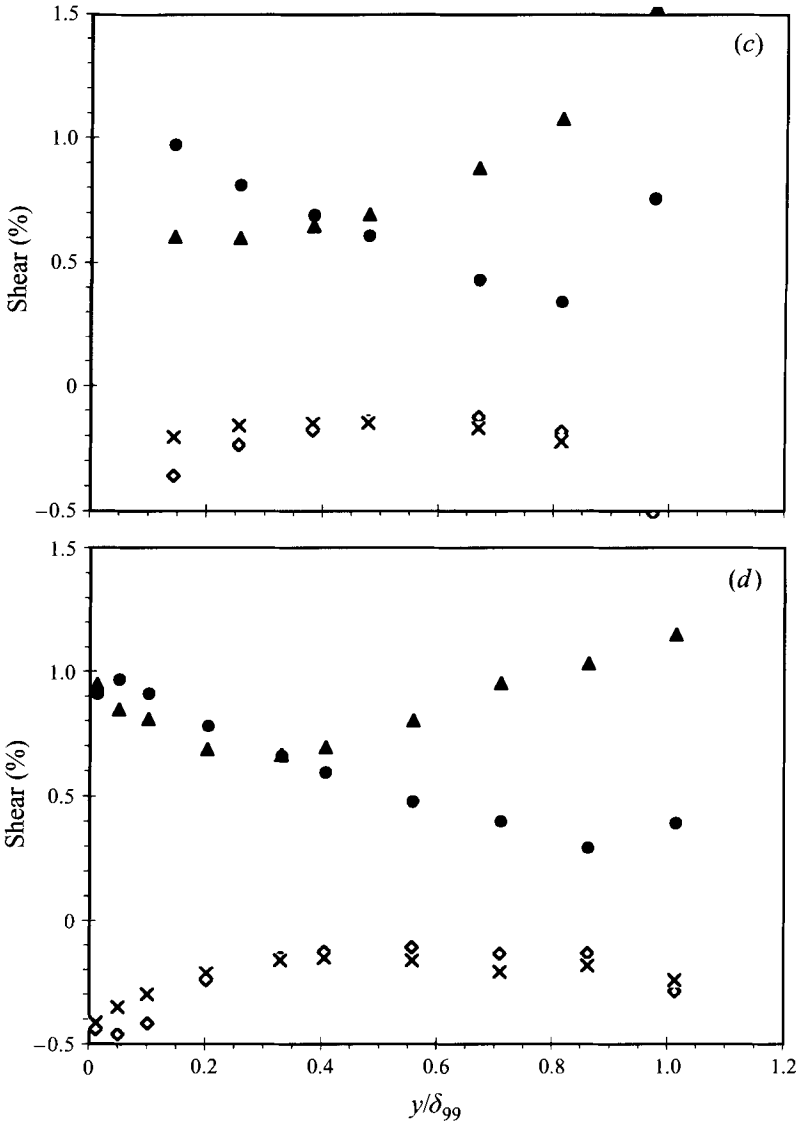

FIGURE 18. Fractional contribution to shear stress of velocity fluctuations $(u(t), v(t))$ from each quadrant, at several streamwise locations. Upstream of separation: (*a*) $\xi = -2.2$, (*b*) $\xi = -1.5$. After reattachment: (*c*) $\xi = 0.7$, (*d*) $\xi = 3.2$. Symbols as in figure 17.

structures in the boundary layer. Furthermore, close to the wall after reattachment, the probabilities of Q1 and Q3 fluctuations approach those of Q2 and Q4, and the contributions of Q1 and Q3 to $-\overline{uv}$ fall towards −50%. That is, the fluctuations in the inner layer are not as highly organized after reattachment as in the unperturbed case, which is consistent with the low levels of the structure parameter there.

5. Discussion

Here, we discuss two important features of the relaxation behaviour after reattachment: first, that the large-scale, outer-layer structure survives the separation bubble to

play a role in the relaxing flow; and second, that the inner-layer flow is quite distorted even at the last measuring station downstream and appears to lack the canonical inner-layer structure there.

That the large-scale structure survives the separation bubble is indicated in several ways. The largest scales are believed to be responsible for turbulence transport across the boundary layer, and during the relaxation the turbulence transport efficiently redistributes the stress peaks present at reattachment to the outer edge of the boundary layer. The profiles of flatness and skewness away from the wall are little altered by separation and reattachment, showing that the outer-scale structure continues to entrain free-stream fluid in much the same way as in an unperturbed layer. The wall flatness increases through separation and remains high in the relaxing flow, implying the continued interaction between the vortex structures and the near-wall fluid, even as the level of fluctuations there (e.g. turbulence kinetic energy) decreases. Quadrant analysis shows that the outer parts of the Q2/Q4 profiles are similar to those in the canonical case. All of these observations point to the presence of large-scale structure over the separation bubble and downstream of reattachment. This is not surprising, because the largest structures are believed to be long-lived under normal circumstances, and in this flow the reduced stretching from the near-wall mean shear appears to reduce the dissipation, which is an important means of weakening or destroying the large-scale structure. The presence of this structure in the relaxing layer is important, because it shows that the outer flow remains boundary-layer-like in spite of the perturbation it experiences over the separation bubble.

In the outer layer, the relaxation process results in all components of the Reynolds-stress tensor reducing towards levels more typical of a canonical boundary layer. The situation is different closer to the wall. By the last measuring station, the $\overline{u^2}$ and $\overline{w^2}$ profiles are fairly flat over the inner third of the boundary layer, while the $\overline{v^2}$ and $-\overline{uv}$ profiles do not change much there and maintain a significant, distinctly non-canonical slope over this region. These differing responses of the $\overline{u^2}$ *vs.* the $\overline{v^2}$ and $-\overline{uv}$ profiles are qualitatively similar to observations downstream of reattachment after strong, geometry-induced separations; see, for example, Chandrsuda & Bradshaw (1981) (reattachment downstream of a backward-facing step) and Ruderich & Fernholz (1986) (reattachment on a lying-T configuration). The flow prior to reattachment is quite different in those works, in both cases separating with a thin laminar boundary layer and including substantial streamwise curvature over the separation region. The slower recovery of $-\overline{uv}$ compared with $\overline{u^2}$ was also seen by Goldberg (1966) in the first measurements of relaxation from this type of separation, although those results have substantial uncertainty near the wall. In that work, the degree of flow reversal was not measured, but the mean-velocity-based correlation of Sandborn & Kline (see for example Kline, Bardina, & Strawn 1983) predicts that the degree of flow reversal is less there than in this work. In these three reattaching flows, then, the histories prior to reattachment are very different from the case studied here, and yet the general shapes of the $\overline{u^2}$ and $-\overline{uv}$ profiles are quite similar. This provides evidence that these profiles are characteristic of reattaching layers and not solely a reflection of the particular upstream history in this study.

This lack of response in the inner-region of the $-\overline{uv}$ profiles is unusual compared with what we might expect from other studies of boundary-layer behaviour after a perturbation. Typically, information about a change in the wall boundary condition is carried away from the wall via the formation of an internal layer which grows into the outer layer as the boundary layer travels downstream. This phenomenon is seen for example in the response to a step change in surface roughness, in wall

temperature, or in wall curvature (many investigations reviewed by Smits & Wood 1985). The growth of the internal layer to the outer edge of the boundary layer does not necessarily signal the end of the recovery (Alving, Smits & Watmuff 1990), but it is the initial relaxation mechanism in a wide variety of perturbed boundary layers and shows that the inner layer is able to regenerate itself when those types of perturbations are removed. In the present study, by contrast, we do not see this type of inner→outer recovery process. Instead, the recovery process occurs largely in the outer layer. The lack of response near the wall cannot be attributed to a slower response time there than in the outer region, since response times are shorter near the wall (see Smits & Wood 1985). The relaxation length $\Delta\xi = 6$ corresponds to $\Delta x/\delta_{99} \sim 20$, a distance over which an internal layer, if formed, could have been expected to grow to the outer edge of the boundary layer (Smits & Wood 1985).

The comparative shapes of the normal-stress profiles are qualitatively similar to those found in isotropic turbulence near a shear-free wall (Thomas & Hancock 1977). The similarities of these flows implies a lack in our reattaching layer of the (non-isotropic) inner-layer structure found in the canonical boundary layer, and this is consistent with the results of Naguib & Wark (1992), who show that in the canonical layer the flat $-\overline{uv}$ profile near the wall is largely the result of inner-layer structure. Thus, the relaxing boundary layer appears to have outer-layer structure with relatively little inner-layer structure, and this configuration prevents the internal-layer response mechanism which is normally found in relaxing boundary layers and which would typically be expected to re-energize the inner layer. This has an important implication for our understanding of inner/outer interactions. Work on large-eddy breakup devices and on convex curvature has shown that the inner layer can maintain itself (produce and transport new turbulence, etc.) when the outer-layer structure is weakened or absent, respectively. Such observations have prompted the speculation that the inner layer is the dominant partner in inner/outer interactions; that the outer layer may modulate but not control the inner layer; and that the inner layer is relatively immune to disturbances of or in the outer layer (see, for example, the review by Robinson 1991*a*). In the present study the boundary layer is perturbed in an unusual way by *enhancing* the outer-layer structure relative to the inner, and the results indicate that the outer layer is here the dominant factor in inner/outer interactions after reattachment. Thus, the balance between the two layers seems more delicate than was previously thought.

6. Concluding remarks

This paper presents the results of an investigation of flow over and downstream of an APG-induced separation bubble. The flow reattaches in a mild adverse pressure gradient. Long after reattachment, the absolute skin friction remains low compared to its level before separation, but this is mostly a reflection of the bulk deceleration experienced by the flow: within about 3 bubble lengths after reattachment the skin friction coefficient based on the *local* free-stream velocity reaches a level typical of a flat-plate turbulent boundary layer having the measured Re_θ.

On the approach to separation, the turbulence quantities show the classic behaviour seen in boundary layers subjected to strong APGs. The Reynolds stresses and production terms decrease near the wall and develop peaks away from the wall. In addition, the net flux of Reynolds stresses increases, presumably because dissipation is decreased as the stretching from the mean shear is reduced. Here, in contrast to the study of DF, normal-stress production does play a significant role, due to the rate

$(\partial()/\partial x)$ at which the boundary layer is being brought to separation. Furthermore, no near-wall plateau in the streamwise Reynolds stress is observed. There is evidence of a decoupling of the production mechanisms of turbulence kinetic energy and Reynolds shear stress, and this may indicate vertical oscillations of the reattaching shear layer.

At the reattachment point, the wall skewness is shown to vanish, as it is known to do at separation. This shows that the sign of the wall skewness reflects the sign of the mean-velocity gradient at the wall.

After reattachment, the outer-layer stresses decay from their elevated levels over the separation bubble. In the inner part of the layer the spanwise component quickly develops a plateau near the wall, and this behaviour is attributed to inviscid reorientation of vorticity. The peaks in both production and turbulence transport are coincident with the peaks in the stress profiles. Production by the normal stresses is no longer significant. The viscous boundary condition increases in importance over the first several bubble lengths, and by $\xi \simeq 3$ dissipation becomes significant.

Far downstream of reattachment, the inner half of the $\overline{u^2}$ and $\overline{w^2}$ profiles become approximately flat, whereas the $\overline{v^2}$ and $-\overline{uv}$ profiles maintain their distinctly peaked shapes with significant slopes near the wall. The outer layer shows evidence of normal boundary-layer structure, but the profile shapes, the structure parameter, and quadrant analysis indicate a lack of near-wall organized structure compared with the canonical layer. The far downstream endurance of this behaviour signals the remarkably slow regrowth of the inner-layer structure. This response is very different from the usual relaxation process after a change in wall boundary condition, in which an internal layer of regenerated stresses would regrow into the outer layer. It seems that this unusual response is the result of the presence of the energetic outer layer, which controls the relaxation process in way not usually seen in boundary-layer recovery.

The first author gratefully acknowledges the support of the Stiftung Luftbrückendank. We thank Dr-Ing. Peter Dengel for sharing his insight into separating boundary layers; Dipl.-Ing. P. M. Wagner for his help in fixing innumerable equipment failures; and Dr-Ing. Wolfgang Baumann for making it possible to work smoothly with half a dozen computer systems in analysing these results. This work was financed by DFG.

REFERENCES

ALVING, A. E. 1988 Boundary layer relaxation from convex curvature. PhD dissertation, Princeton University (T-1816, Mechanical and Aerospace Engineering).

ALVING, A. E. & FERNHOLZ, H. H. 1995 Mean-velocity scaling in and around a mild, turbulent separation bubble. *Phys. Fluids* **7**, 1956–1969 (referred to herein as AF).

ALVING, A. E., SMITS, A. J. & WATMUFF, J. H. 1990 Turbulent boundary layer relaxation from convex curvature. *J. Fluid Mech.* **211**, 529–556.

BRADBURY, L. J. S. & CASTRO, I. P. 1971 A pulsed-wire technique for velocity measurements in highly turbulent flows. *J. Fluid Mech.* **49**, 657–691.

CHANDRSUDA, C. & BRADSHAW, P. 1981 Turbulence structure of a reattaching mixing layer. *J. Fluid Mech.* **110**, 171–194.

CHERRY, N. J., HILLIER, R. & LATOUR, M. E. M. P. 1984 Unsteady measurements in a separated and reattaching flow. *J. Fluid Mech.* **144**, 13–46.

DENGEL, P. 1992 Über die Struktur und die Sensibilität einer inkompressiblen turbulenten Grenzschicht am Rande der Ablösung (Concerning the structure and sensitivity of an incompressible turbulent boundary layer close to separation). Dissertation, Technische Universität Berlin D83.

DENGEL, P. & FERNHOLZ, H. H. 1989 Generation of and measurements in a turbulent boundary layer with zero skin friction. In *Advances in Turbulence 2*, (ed. H. H. Fernholz & H. E. Fielder), pp. 432–437. Springer (referred to herein as DF).

DENGEL, P. & FERNHOLZ, H. H. 1990 An experimental investigation of an incompressible turbulent boundary layer in the vicinity of separation. *J. Fluid Mech.* **212**, 615–636.

DRIVER, D. M. 1991 Reynolds shear stress measurements in a separated boundary layer flow. *AIAA Paper* 91–1787.

DURBIN, P. A. & BELCHER, S. E. 1992 Scaling of adverse-pressure-gradient turbulent boundary layers. *J. Fluid Mech.* **238**, 699–722.

FERNHOLZ, H. H. 1993 Near-wall phenomena in turbulent separated flows. *Acta Mechanica* [suppl.] **4**, 1–8.

GOLDBERG, P. 1966 Upstream history and apparent stress in turbulent boundary layers. *MIT Gas Turbine Rep.* 85.

JAROCH, M. 1985 Development and testing of pulsed-wire probes for measuring fluctuating quantities in highly turbulent flows. *Exps. Fluids* **3**, 315–322.

JOHANSSON, A. V. & ALFREDSSON, P. H. 1982 On the structure of turbulent channel flow. *J. Fluid Mech.* **122**, 295–314.

KLINE, S. J., BARDINA, J. G. & STRAWN, R. C. 1983 Correlation of the detachment of two-dimensional turbulent boundary layers. *AIAA J.* **21**, 68–73.

MELNIK, R. E. 1989 An asymptotic theory of turbulent separation. *Computers Fluids* **17**, 165–184.

MELNIK, R. E. 1991 Some applications of asymptotic theory to turbulent flow. *AIAA Paper* 91–0220.

MENTER, F. R. 1992 Performance of popular turbulence models for attached and separated adverse pressure gradient flows. *AIAA J.* **30**, 2066–2072.

MOSES, H. L. 1964 The behaviour of turbulent boundary layers in adverse pressure gradients. PhD dissertation; *MIT Gas Turbine Rep.* 73.

NAGUIB, A. M. & WARK, C. E. 1992 An investigation of wall-layer dynamics using a combined temporal filtering and correlation technique. *J. Fluid Mech.* **243**, 541–560.

PERRY, A. E. & SCHOFIELD, W. H. 1973 Mean velocity and shear stress distributions in turbulent boundary layers. *Phys. Fluids* **16**, 2068–2074.

ROBINSON, S. K. 1991*a* Coherent motions in the turbulent boundary layer. *Ann. Rev. Fluid Mech.* **23**, 601–639.

ROBINSON, S. K. 1991*b* The kinematics of turbulent boundary layer structure. *NASA–TM* 103859.

RUDERICH, R. & FERNHOLZ, H. H. 1986 An experimental investigation of a turbulent shear flow with separation, reverse flow, and reattachment. *J. Fluid Mech.* **163**, 283–322.

SCHLICHTING, H. 1979 *Boundary Layer Theory.* McGraw–Hill.

SCHALAU, B. DENGEL, P. & THIELE, F. 1989 Computation of turbulent boundary-layer flow with separation – a critical evaluation of parameters influencing the results. In *Advances in Turbulence 2* (ed. H. H. Fernholz & H. E. Fiedler), pp. 432–437. Springer.

SCHOFIELD, W. H. 1981 Equilibrium boundary layers in moderate to strong adverse pressure gradient. *J. Fluid Mech.* **113**, 91–122.

SCHOFIELD, W. H. 1986 Two-dimensional separating turbulent boundary layers. *AIAA J.* **24**, 1611–1620.

SHILOH, K., SHIVAPRASAD, B. G. & SIMPSON, R. L. 1981 The structure of a separating turbulent boundary layer. Part 3. Transverse velocity measurements. *J. Fluid Mech.* **113**, 75–90.

SIMPSON, R. L., CHEW, Y.-T. & SHIVAPRASAD, B. G. 1981*a* The structure of a separating turbulent boundary layer. Part 1. Mean flow and Reynolds stresses. *J. Fluid Mech.* **113**, 23–51.

SIMPSON, R. L., CHEW, Y.-T. & SHIVAPRASAD, B. G. 1981*b* The structure of a separating turbulent boundary layer. Part 2. Higher-order turbulence results. *J. Fluid Mech.* **113**, 53–73.

SMITS, A. J. & WOOD, D. H. 1985 The response of turbulent boundary layers to sudden perturbations. *Ann. Rev. Fluid Mech.* **17**, 321–358.

SPANGENBERG, W. G., ROWLAND, W. R. & MEASE, N. R. 1967 Measurements in a turbulent boundary layer maintained in a nearly separation condition. In *Fluid Mechanics of Internal Flow* (ed. G. Sovran), pp. 110–151. Elsevier.

STRATFORD, B. S. 1959*a* The prediction of separation of the turbulent boundary layer. *J. Fluid Mech.* **5**, 1–16.

STRATFORD, B. S. 1959*b* An experimental flow with zero skin friction throughout its region of pressure rise. *J. Fluid Mech.* **5**, 17–35.

THOMAS, N. H. & HANCOCK, P. E. 1977 Grid turbulence near a moving wall. *J. Fluid Mech.* **82**, 481–496.

TOWNSEND, A. A. 1961 Equilibrium layers and wall turbulence. *J. Fluid Mech.* **11**, 97–120.

WAGNER, P. M. 1986 Entwicklung eines verbesserten Pulsdrahtanemometers zur Erfassung von Geschwindigkeiten und Korrelationen in turbulenten Strömungen (The development of an improved pulsed-wire anemometer to measure speeds and correlations in turbulent flows). Diplomarbeit (thesis), Technische Universität, Berlin, Germany.